

The Air Pollution Model (TAPM) Version 2. Part 1: Technical Description

Peter Hurley



Hurley, Peter, 1963- .

The air pollution model (TAPM) version 2. Part 1, Technical description.

ISBN 0 643 06651 9.

1. Air - Pollution - Mathematical models. 2. Air - Pollution - Measurement. 3. Air - Pollution - Meteorological aspects. I. CSIRO. Division of Atmospheric Research. II. Title. (Series : CSIRO Atmospheric Research technical paper ; no. 55).

551.51

In accordance with the Copyright Act 1968 a copy of each book published must be lodged with the National Library and respective deposit libraries in each state.

The Air Pollution Model (TAPM) Version 2. Part 1: Technical Description

Peter Hurley
CSIRO Atmospheric Research
Private Bag 1, Aspendale,
Vic 3195, Australia

Abstract

Air pollution predictions for environmental impact assessments usually use Gaussian plume/puff models driven by observationally-based meteorological inputs. An alternative approach is to use prognostic meteorological and air pollution models, which have many advantages over the Gaussian approach and are now becoming a viable tool for performing year-long simulations. Continuing rapid increases in computing power are bringing this approach to the PC. This report provides a comprehensive technical description of the newly enhanced prognostic model called The Air Pollution Model (TAPM).

1 Introduction

Air pollution models that can be used to predict hour by hour pollution concentrations for periods of up to a year, are generally semi-empirical/analytic approaches based on Gaussian plumes or puffs. These models typically use either a simple surface based meteorological file or a diagnostic wind field model based on available observations. The Air Pollution Model (TAPM) is different to these approaches in that it solves approximations to the fundamental fluid dynamics and scalar transport equations to predict meteorology and pollutant concentration for a range of pollutants important for air pollution applications. TAPM consists of coupled prognostic meteorological and air pollution concentration components, eliminating the need to have site-specific meteorological observations. Instead, the model predicts the flows important to local-scale air pollution, such as sea breezes and terrain-induced flows, against a background of larger-scale meteorology provided by synoptic analyses.

The meteorological component of TAPM is an incompressible, non-hydrostatic, primitive equation model with a terrain-following vertical coordinate for three-dimensional simulations. The model solves the momentum equations for horizontal wind components, the incompressible continuity equation for vertical velocity, and scalar equations for potential virtual temperature and specific humidity of water vapour, cloud water and rain water. The Exner pressure function is split into hydrostatic and non-hydrostatic components, and a Poisson equation is solved for the non-hydrostatic component. Explicit cloud micro-physical processes are included. The turbulence terms in these equations have been determined by solving equations for turbulence kinetic energy and eddy dissipation rate, and then using these values in representing the vertical fluxes by a gradient diffusion approach, including a counter-gradient term for heat flux. A vegetative canopy and soil scheme is used at the surface, while radiative fluxes, both at the surface and at upper levels, are also included.

The air pollution component of TAPM, which uses the predicted meteorology and turbulence from the meteorological component, consists of four modules. The Eulerian Grid Module

(EGM) solves prognostic equations for concentration and for cross-correlation of concentration and virtual potential temperature. The Lagrangian Particle Module (LPM) can be used to represent near-source dispersion more accurately. The Plume Rise Module is used to account for plume momentum and buoyancy effects for point sources. The Building Wake Module allows plume rise in EGM or LPM mode, and dispersion in LPM mode, to include wake effects on meteorology and turbulence. The model also includes gas-phase photochemical reactions based on the Generic Reaction Set, and gas- and aqueous-phase chemical reactions for sulfur dioxide and particles. Wet and dry deposition effects are also included.

This paper describes the technical details of the modelling approach, including the meteorological component in Section 2 and the pollution component in Section 3. Section 4 outlines the numerical methods used in the model. Changes in TAPM V2.0 from the previous major releases of the model (V1.0 and V1.4) are summarised in the Appendix. Part 2 of this paper (Hurley *et al.*, 2002) presents a summary of some verification studies performed with TAPM V2.0.

2 Meteorological component

The meteorological component of TAPM is an incompressible, optionally non-hydrostatic, primitive equation model with a terrain-following vertical coordinate for three-dimensional simulations. It includes parameterisations for cloud/rain micro-physical processes, turbulence closure, urban/vegetative canopy and soil, and radiative fluxes. The model solution for winds, potential virtual temperature and specific humidity, is weakly nudged with a 24-hour e-folding time towards the synoptic-scale input values of these variables.

Note that the horizontal model domain size should be restricted in size to less than about 1000 km x 1000 km, as the model equations neglect the curvature of the earth and assume a uniform distance grid spacing across the domain.

2.1 Base meteorological variables

The mean wind is determined for the horizontal components u and v (m s^{-1}) from the momentum equations and the terrain following vertical velocity $\dot{\sigma}$ (m s^{-1}) from the continuity equation. Potential virtual temperature θ_v (K) is determined from an equation combining conservation of heat and water vapour. The Exner pressure function $\pi = \pi_H + \pi_N$ ($\text{J kg}^{-1} \text{K}^{-1}$) is determined from the sum of the hydrostatic component π_H and non-hydrostatic component π_N (see Section 2.2). The equations for these variables are as follows

$$\frac{du}{dt} = F(u) + \frac{\partial \bar{w}' u'}{\partial \sigma} \frac{\partial \sigma}{\partial z} - \theta_v \left(\frac{\partial \pi}{\partial x} + \frac{\partial \pi}{\partial \sigma} \frac{\partial \sigma}{\partial x} \right) + fv - N_s(u - u_s) \quad (1)$$

$$\frac{dv}{dt} = F(v) + \frac{\partial \bar{w}' v'}{\partial \sigma} \frac{\partial \sigma}{\partial z} - \theta_v \left(\frac{\partial \pi}{\partial y} + \frac{\partial \pi}{\partial \sigma} \frac{\partial \sigma}{\partial y} \right) - fu - N_s(v - v_s) \quad (2)$$

$$\frac{\partial \dot{\sigma}}{\partial \sigma} = - \left(\frac{\partial u}{\partial x} + \frac{\partial v}{\partial y} \right) + u \frac{\partial}{\partial \sigma} \left(\frac{\partial \sigma}{\partial x} \right) + v \frac{\partial}{\partial \sigma} \left(\frac{\partial \sigma}{\partial y} \right) \quad (3)$$

$$\frac{d\theta_v}{dt} = F(\theta_v) + \overline{\frac{\partial w' \theta_v}{\partial \sigma}} \frac{\partial \sigma}{\partial z} + S_{\theta_v} - N_s (\theta_v - \theta_{vs}) \quad (4)$$

$$\frac{\partial \pi_H}{\partial \sigma} = -\frac{g}{\theta_v} \left(\frac{\partial \sigma}{\partial z} \right)^{-1} \quad (5)$$

where

t = time (s),

x, y, σ = the components of the coordinate system (m),

$$\sigma = z_T \left(\frac{z - z_s}{z_T - z_s} \right)$$

z = cartesian vertical coordinate (m),

z_T = height of model top (m),

z_s = terrain height (m),

$$\frac{d\phi}{dt} \equiv \frac{\partial \phi}{\partial t} + u \frac{\partial \phi}{\partial x} + v \frac{\partial \phi}{\partial y} + \dot{\sigma} \frac{\partial \phi}{\partial \sigma},$$

$F(\phi)$ = horizontal filtering of ϕ (see Section 4.3),

$\overline{w' \phi'}$ = vertical flux of ϕ (see Section 2.4),

f = Coriolis parameter ($4\pi_c \sin(lat)/(24 \times 3600)$) (s⁻¹),

$\pi_c = 3.14159265$,

lat = latitude (°),

u_s, v_s, θ_{vs} = large scale synoptic winds and potential virtual temperature,

N_s = large scale nudging coefficient (1/(24 × 3600)),

$$S_{\theta_v} = \frac{\theta_v}{T} \left(\frac{\partial T}{\partial t} \right)_{RADIATION} - \frac{\lambda}{c_p} S_{q_v} \quad (\text{see Sections 2.3 and 2.5}),$$

T = temperature (K),

g = gravitational constant (9.81 m s⁻²),

λ = latent heat of vaporisation of water (2.5×10^6 J kg⁻¹),

c_p = specific heat at constant pressure (1006 J kg⁻¹ K⁻¹),

$$\frac{\partial \sigma}{\partial x} = \left(\frac{\sigma - z_T}{z_T - z_s} \right) \frac{\partial z_s}{\partial x}, \quad \frac{\partial \sigma}{\partial y} = \left(\frac{\sigma - z_T}{z_T - z_s} \right) \frac{\partial z_s}{\partial y}, \quad \frac{\partial \sigma}{\partial z} = \left(\frac{z_T}{z_T - z_s} \right).$$

2.2 Non-hydrostatic pressure

The optional non-hydrostatic component of the Exner pressure function π_N is determined by taking spatial derivatives of the three momentum equations and the time derivative of the continuity equation, and then eliminating all time derivatives in the continuity equation by substitution. The following assumes all products of Coriolis terms and terrain gradients, and all turbulence and synoptic variation terms, can be neglected. The resultant equation for π_N is

$$\begin{aligned} & \frac{\partial^2 \pi_N}{\partial x^2} + 2 \frac{\partial \sigma}{\partial x} \frac{\partial^2 \pi_N}{\partial x \partial \sigma} + \frac{\partial^2 \pi_N}{\partial y^2} + 2 \frac{\partial \sigma}{\partial y} \frac{\partial^2 \pi_N}{\partial y \partial \sigma} + \left(\frac{\partial \sigma}{\partial z} \right)^2 \frac{\partial^2 \pi_N}{\partial \sigma^2} \\ & + C_x \frac{\partial \pi_N}{\partial x} + C_y \frac{\partial \pi_N}{\partial y} + C_\sigma \frac{\partial \pi_N}{\partial \sigma} = R_\pi, \end{aligned} \quad (6)$$

with coefficients

$$\begin{aligned} C_x &= \frac{1}{\theta_v} \left(\frac{\partial \theta_v}{\partial x} + \frac{\partial \theta_v}{\partial \sigma} \frac{\partial \sigma}{\partial x} \right), \quad C_y = \frac{1}{\theta_v} \left(\frac{\partial \theta_v}{\partial y} + \frac{\partial \theta_v}{\partial \sigma} \frac{\partial \sigma}{\partial y} \right), \\ C_\sigma &= \frac{1}{\theta_v} \left(\frac{\partial \theta_v}{\partial x} \frac{\partial \sigma}{\partial x} + \frac{\partial \theta_v}{\partial y} \frac{\partial \sigma}{\partial y} + \frac{\partial \theta_v}{\partial \sigma} \left(\frac{\partial \sigma}{\partial z} \right)^2 \right) + \frac{\partial^2 \sigma}{\partial x^2} + \frac{\partial^2 \sigma}{\partial y^2}, \\ R_\pi &= \frac{1}{\theta_v} \left(\frac{\partial R_u}{\partial x} + \frac{\partial R_v}{\partial y} + \frac{\partial R_\sigma}{\partial \sigma} - R_u \frac{\partial}{\partial \sigma} \left(\frac{\partial \sigma}{\partial x} \right) - R_v \frac{\partial}{\partial \sigma} \left(\frac{\partial \sigma}{\partial y} \right) \right), \\ R_u &= -u \frac{\partial u}{\partial x} - v \frac{\partial u}{\partial y} - \dot{\sigma} \frac{\partial u}{\partial \sigma} + fv - \theta_v \frac{\partial \pi_H}{\partial x} + g \frac{\partial \sigma}{\partial x} \left(\frac{\partial \sigma}{\partial z} \right)^{-1}, \\ R_v &= -u \frac{\partial v}{\partial x} - v \frac{\partial v}{\partial y} - \dot{\sigma} \frac{\partial v}{\partial \sigma} - fu - \theta_v \frac{\partial \pi_H}{\partial y} + g \frac{\partial \sigma}{\partial y} \left(\frac{\partial \sigma}{\partial z} \right)^{-1}, \\ R_\sigma &= -u \frac{\partial \dot{\sigma}}{\partial x} - v \frac{\partial \dot{\sigma}}{\partial y} - \dot{\sigma} \frac{\partial \dot{\sigma}}{\partial \sigma} - \theta_v \left(\frac{\partial \pi_H}{\partial x} \frac{\partial \sigma}{\partial x} + \frac{\partial \pi_H}{\partial y} \frac{\partial \sigma}{\partial y} \right) \\ & + u^2 \frac{\partial^2 \sigma}{\partial x^2} + 2uv \frac{\partial^2 \sigma}{\partial x \partial y} + v^2 \frac{\partial^2 \sigma}{\partial y^2} + 2\dot{\sigma} \left(u \frac{\partial}{\partial \sigma} \left(\frac{\partial \sigma}{\partial x} \right) + v \frac{\partial}{\partial \sigma} \left(\frac{\partial \sigma}{\partial y} \right) \right), \end{aligned}$$

and

$$\begin{aligned} \frac{\partial}{\partial \sigma} \left(\frac{\partial \sigma}{\partial x} \right) &= \left(\frac{1}{z_T - z_s} \right) \frac{\partial z_s}{\partial x}, \quad \frac{\partial}{\partial \sigma} \left(\frac{\partial \sigma}{\partial y} \right) = \left(\frac{1}{z_T - z_s} \right) \frac{\partial z_s}{\partial y}, \\ \frac{\partial^2 \sigma}{\partial x^2} &= \left(\frac{\sigma - z_T}{z_T - z_s} \right) \frac{\partial^2 z_s}{\partial x^2}, \quad \frac{\partial^2 \sigma}{\partial x \partial y} = \left(\frac{\sigma - z_T}{z_T - z_s} \right) \frac{\partial^2 z_s}{\partial x \partial y}, \quad \frac{\partial^2 \sigma}{\partial y^2} = \left(\frac{\sigma - z_T}{z_T - z_s} \right) \frac{\partial^2 z_s}{\partial y^2}. \end{aligned}$$

2.3 Water and micro-physics

Conservation equations are solved for specific humidity (kg kg^{-1}) $q = q_v + q_c$ and q_r representing the sum of water vapour and cloud water, and rain water respectively

$$\frac{dq}{dt} = \frac{\partial \overline{u'q'}}{\partial x} + \frac{\partial \overline{v'q'}}{\partial y} + \frac{\partial \overline{w'q'}}{\partial z} \frac{\partial \sigma}{\partial z} + S_{q_v} + S_{q_c} - N_s (q - q_s) \quad (7)$$

$$\frac{dq_r}{dt} = \frac{\partial \overline{u'q'_r}}{\partial x} + \frac{\partial \overline{v'q'_r}}{\partial y} + \frac{\partial \overline{w'q'_r}}{\partial z} \frac{\partial \sigma}{\partial z} + S_{q_r} - V_T \frac{\partial q_r}{\partial \sigma} \frac{\partial \sigma}{\partial z} \quad (8)$$

with

$S_{q_v}, S_{q_c}, S_{q_r}$ = micro-physical source terms,

q_s = synoptic scale specific humidity of water vapour plus cloud water,

V_T = rainfall terminal velocity,

and the specific humidity of water vapour q_v and the saturated specific humidity q_{vs} determined from

$$q_v = \min(q, q_{vs}),$$

$$q_{vs} = \frac{0.622e_{vs}}{(p - 0.378e_{vs})},$$

p = pressure (Pa), and

$$e_{vs} = 610 \exp\left(\frac{\lambda}{R_v} \left(\frac{1}{273.15} - \frac{1}{T}\right)\right).$$

Micro-physics is based on Katzfey and Ryan (1997) for warm rain (ice processes are generally important only for temperatures less than -10°C), and includes bulk parameterisations for condensation of water vapour, evaporation of cloud water and rain water, auto-conversion and collection of cloud water to form rain water, and an expression for the rainfall terminal velocity.

The source terms in the water conservation equations are determined by

$$S_{q_v} = -P_{VC} - P_{VR}, \quad S_{q_c} = P_{VC} - P_{CR}, \quad S_{q_R} = P_{CR} + P_{VR},$$

where

$$\begin{aligned} P_{VC} &= \left(\frac{q_v - q_{vs}}{\Delta t} \right) \left(1 + \frac{\lambda}{c_p} \frac{dq_{vs}}{dT} \right)^{-1} \\ P_{CR} &= \frac{0.057g}{\mu} H(q_c - 0.0001) \left(\frac{\rho^4 q_c^7}{N_c \rho_w} \right)^{1/3} + 0.884 q_c q_R \left(\frac{g \lambda_R \rho}{\rho_w} \right)^{1/2} \\ P_{VR} &= \min(0, \frac{q_v}{q_{vs}} - 1) \frac{q_R \lambda_R^2}{\rho_w} \left(\frac{0.5 + \frac{0.349}{\mu^{1/2}} \left(\frac{\rho_w g \rho}{\lambda_R^3} \right)^{1/4}}{\frac{\lambda^2}{KR_v T^2} + \frac{R_v T}{e_{vs} D_v}} \right) \end{aligned}$$

where H is the Heaviside function.

The rainfall terminal velocity is determined from $V_T = -2.13 \left(\frac{g \rho_w}{\lambda_R \rho} \right)^{1/2}$.

Constants are

$$N_c = 5 \times 10^7 \text{ m}^{-3}, \quad \lambda_R = 3846 \text{ m}^{-1}, \quad \rho_w = 1000 \text{ kg m}^{-3}, \quad R_v = 461.5 \text{ J kg}^{-1} \text{ K}^{-1},$$

$$\mu = 1.8 \times 10^{-5} \text{ kg m}^{-1} \text{ s}^{-1}, \quad K = 0.025 \text{ J m}^{-1} \text{ s}^{-1}, \quad D_v = 2.5 \times 10^{-5} \text{ m}^2 \text{ s}^{-1}.$$

Calculation of the precipitation rate (m s^{-1}) at the surface is from $P = \frac{\rho}{\rho_w} V_T q_R(0)$, where

$q_R(0)$ is the amount of rain reaching the ground.

In order to account for the lack of cloud water information in the synoptic analyses, we enhance the synoptic total water used in the model, by multiplying the synoptic-scale relative humidity by the following factor:

$$F_{\text{synoptic_water}} = \max\left(1, 1 + 2\left(\frac{RH_{\text{synoptic}} - RH_0}{100 + RH_0}\right)\right),$$

where RH_{synoptic} is the original synoptic-scale relative humidity and $RH_0 = 80\%$ is the threshold value above which enhancement is carried out. This parameterisation results in no change to the synoptic-scale relative humidity for $RH_{\text{synoptic}} < 80\%$ and gives an enhanced value of 100% when $RH_{\text{synoptic}} = 90\%$. This approach is consistent with cloud cover parameterisations used in global and synoptic scale models (e.g. see Rikus, 1993).

2.4 Turbulence and diffusion

Turbulence closure in the mean equations uses a gradient diffusion approach, which depends on a diffusion coefficient K and gradients of mean variables. Using Cartesian tensor notation, the fluxes are

$$\overline{u'_i u'_j} = \frac{2}{3} E \delta_{ij} - K \left(\frac{\partial u_i}{\partial x_j} + \frac{\partial u_j}{\partial x_i} \right),$$

$$\overline{u'_i \theta'_v} = -K \left(\frac{\partial \theta_v}{\partial x_i} - \gamma_{\theta_v} \right),$$

$$\overline{u'_i \phi'} = -2.5K \frac{\partial \phi}{\partial x_i},$$

where

i, j are subscripts for the three coordinate directions (i.e. $i = 1, 2, 3$ for x, y, z respectively),

u_i, u_j represent velocities,

$$\delta_{ij} = \begin{cases} 1 & \text{if } i = j, \\ 0 & \text{otherwise.} \end{cases}$$

$\gamma_{\theta_v} = 0.00065 \text{ K m}^{-1}$ from Deardorff (1966),

ϕ represents a scalar.

The scalar diffusion coefficient of 2.5 used above is based on an analysis of the second order closure equations from Andren (1990), with constants from Rodi (1985).

The turbulence scheme used to calculate K is the standard $E-\varepsilon$ model in three-dimensional terrain-following coordinates, with constants for the eddy dissipation rate equation derived from the analysis of Duynkerke (1988). The model solves prognostic equations for the turbulence kinetic energy (E) and the eddy dissipation rate (ε)

$$\frac{dE}{dt} = \frac{\partial}{\partial x} \left(K \frac{\partial E}{\partial x} \right) + \frac{\partial}{\partial y} \left(K \frac{\partial E}{\partial y} \right) + \left(\frac{\partial \sigma}{\partial z} \right)^2 \frac{\partial}{\partial \sigma} \left(K \frac{\partial E}{\partial \sigma} \right) + P_s + P_b - \varepsilon, \quad (9)$$

$$\begin{aligned} \frac{d\epsilon}{dt} = & \frac{\partial}{\partial x} \left(K \frac{\partial \epsilon}{\partial x} \right) + \frac{\partial}{\partial y} \left(K \frac{\partial \epsilon}{\partial y} \right) + \left(\frac{\partial \sigma}{\partial z} \right)^2 \frac{\partial}{\partial \sigma} \left(c_{\epsilon 0} K \frac{\partial \epsilon}{\partial \sigma} \right) \\ & + \frac{\epsilon}{E} (c_{\epsilon 1} \max(P_s, P_s + P_b) - c_{\epsilon 2} \epsilon), \end{aligned} \quad (10)$$

where

$$\begin{aligned} P_s = & 2K \left(\left(\frac{\partial u}{\partial x} + \frac{\partial u}{\partial \sigma} \frac{\partial \sigma}{\partial x} \right)^2 + \left(\frac{\partial v}{\partial y} + \frac{\partial v}{\partial \sigma} \frac{\partial \sigma}{\partial y} \right)^2 + \left(\frac{\partial w}{\partial \sigma} \frac{\partial \sigma}{\partial z} \right)^2 \right) \\ & + K \left(\left(\frac{\partial u}{\partial y} + \frac{\partial u}{\partial \sigma} \frac{\partial \sigma}{\partial y} + \frac{\partial v}{\partial x} + \frac{\partial v}{\partial \sigma} \frac{\partial \sigma}{\partial x} \right)^2 \right) \\ & + K \left(\left(\frac{\partial u}{\partial \sigma} \frac{\partial \sigma}{\partial z} + \frac{\partial w}{\partial x} + \frac{\partial w}{\partial \sigma} \frac{\partial \sigma}{\partial x} \right)^2 + \left(\frac{\partial v}{\partial \sigma} \frac{\partial \sigma}{\partial z} + \frac{\partial w}{\partial y} + \frac{\partial w}{\partial \sigma} \frac{\partial \sigma}{\partial y} \right)^2 \right), \end{aligned}$$

$$P_b = -\frac{g}{\theta_v} K \left(\frac{\partial \theta_v}{\partial \sigma} \frac{\partial \sigma}{\partial z} - \gamma_{\theta_v} \right),$$

$$\text{with } w = \left(\frac{\partial \sigma}{\partial z} \right)^{-1} \left(\dot{\sigma} - u \frac{\partial \sigma}{\partial x} - v \frac{\partial \sigma}{\partial y} \right),$$

$$\text{and } K = c_m \frac{E^2}{\epsilon}, \quad c_m = 0.09, \quad c_{\epsilon 0} = 0.69, \quad c_{\epsilon 1} = 1.46, \quad \text{and} \quad c_{\epsilon 2} = 1.83.$$

As an alternative to Equation (10) the model has an option to use a diagnostic eddy dissipation rate based on Duynkerke and Driedonks (1987). In this approach,

$$\epsilon = c_m^{3/4} \frac{E^{3/2}}{l},$$

$$l = \min(l_b, l_s),$$

$$l_b = \left(\frac{\phi_M}{kz} + \frac{1}{l_o} \right)^{-1},$$

$$l_s = 0.36 E^{1/2} \left(\frac{g}{\theta_v} \frac{\partial \theta_v}{\partial z} \right)^{-1/2},$$

$$l_o = 0.3 \frac{\int E z dz}{\int E dz},$$

ϕ_M = surface layer similarity function (see Section 2.6.4),

k = von Karman constant (0.4).

2.5 Radiation

2.5.1 Clear-sky

Radiation at the surface is used for the computation of surface boundary conditions and scaling variables (see later), with the clear-sky incoming short-wave component from Mahrer and Pielke (1977),

$$R_{sw(clear\text{-}sky)}^{in} = \begin{cases} (a_g - a_w(z_s))S_{slope}S_o \cos \chi; & \text{for } \cos \chi > 0 \\ 0; & \text{for } \cos \chi \leq 0 \end{cases}$$

and the clear-sky incoming long-wave component from Dilley and O'Brien (1999),

$$R_{lw(clear\text{-}sky)}^{in} = \left(59.38 + 113.7 \left(\frac{T(\sigma_1)}{273.15} \right)^6 + 96.96 \left(\frac{r(\sigma_1)}{25} \right)^{1/2} \right) \cos \alpha,$$

with

$$a_g = 0.485 + 0.515 \left(1.014 - 0.16 / \sqrt{\cos \chi} \right)$$

$$a_w(\sigma) = 0.039 \left(\frac{r(\sigma)}{\cos \chi} \right)^{0.3},$$

$r(\sigma) = \int_{\sigma}^{z_T} \rho q d\sigma$ is the column water vapour amount (kg m^{-2} or mm) between z_T and σ ,

χ is the zenith angle, and S_o is the solar constant (1367 W m^{-2}).

The solar declination, zenith, and terrain slope angles are calculated using

$$\sin \delta_s = \sin(23.5\pi_c / 180) \sin(2\pi_c day / 365),$$

$$\cos \chi = \cos(lat) \cos \delta_s \cos(\pi_c (hour - 12) / 12) + \sin(lat) \sin \delta_s,$$

$$S_{slope} = \frac{\cos i}{\cos \chi}, \quad \cos i = \cos \alpha \cos \chi + \sin \alpha \sin \chi \cos(\beta - \eta),$$

$$\alpha = \tan^{-1} \left(\left(\frac{\partial z_s}{\partial x} \right)^2 + \left(\frac{\partial z_s}{\partial y} \right)^2 \right), \quad \eta = \tan^{-1} \left(\left(\frac{\partial z_s}{\partial y} \right) \left(\frac{\partial z_s}{\partial x} \right)^{-1} \right) - \frac{\pi_c}{2},$$

$$\beta = \sin^{-1} (\cos \delta_s \sin(\pi_c (hour - 12) / 12) / \sin \chi),$$

lat = latitude, day = day of year ($1 \equiv 21$ March),

$hour$ = hour of day (24 hour clock), $\pi_c = 3.14159265$.

The effects of water vapour and carbon dioxide on atmospheric heating/cooling rates for both short-wave and long-wave radiation follow Mahrer and Pielke (1977)

$$\left. \frac{\partial T}{\partial t} \right|_{RADIATION(clear\text{-}sky)} = \frac{1}{\rho c_p} \left(-S_o \cos \chi \frac{\partial a_w}{\partial \sigma} \frac{\partial \sigma}{\partial z} \right. \\ \left. - \sigma_{SB} \frac{\partial \varepsilon \uparrow}{\partial \sigma} \frac{\partial \sigma}{\partial z} \left((T(\sigma))^4 - (T(0))^4 \right) - \sigma_{SB} \frac{\partial \varepsilon \downarrow}{\partial \sigma} \frac{\partial \sigma}{\partial z} \left((T(z_T))^4 - (T(\sigma))^4 \right) \right)$$

with

$$a_w(\sigma) = 0.039 \left(\frac{r(\sigma)}{\cos \chi} \right)^{0.3},$$

$$r(\sigma) = \int_{\sigma}^{z_T} \rho q_v d\sigma,$$

and emissivity $\varepsilon = \varepsilon_{q_v} + \varepsilon_{CO_2}$ either integrated upwards ($\varepsilon \uparrow$) or downwards ($\varepsilon \downarrow$) with

$$\varepsilon_{q_v} = \begin{cases} 0.113 \log_{10}(1 + 12.6 \delta P), & \text{for } \log_{10} \delta P \leq -4 \\ 0.104 \log_{10} \delta P + 0.440, & \text{for } -4 < \log_{10} \delta P \leq -3 \\ 0.121 \log_{10} \delta P + 0.491, & \text{for } -3 < \log_{10} \delta P \leq -1.5 \\ 0.146 \log_{10} \delta P + 0.527, & \text{for } -1.5 < \log_{10} \delta P \leq -1 \\ 0.161 \log_{10} \delta P + 0.542, & \text{for } -1 < \log_{10} \delta P \leq 0 \\ 0.136 \log_{10} \delta P + 0.542, & \text{for } \log_{10} \delta P > 0 \end{cases}$$

$$\varepsilon_{CO_2} = 0.185 (1 - \exp(-0.39(\delta H)^{0.4})),$$

$$\delta P = 0.1 r(\sigma) = \begin{cases} 0.1 \int_{\sigma}^{\sigma} \rho q_v d\sigma, & \text{for } \varepsilon \uparrow \\ 0.1 \int_{\sigma}^{z_S} \rho q_v d\sigma, & \text{for } \varepsilon \downarrow \end{cases},$$

$$\delta H = \begin{cases} 0.252(p_S - p)/100, & \text{for } \varepsilon \uparrow \\ 0.252(p - p_T)/100, & \text{for } \varepsilon \downarrow \end{cases},$$

where

p is pressure (hPa),

subscripts S and T indicate the ground surface or model top respectively,

and $\sigma_{SB} = 5.67 \times 10^{-8} \text{ W m}^{-2} \text{ K}^{-4}$ is the Stefan Boltzman constant.

2.5.2 Cloudy sky

The clear-sky incoming radiation components from the previous section are modified for liquid water effects using an approach based on Stephens (1978). The method assumes clear and cloudy sky contributions can be treated separately.

The incoming short-wave radiation is

$$R_{sw}^{in}(\sigma) = R_{sw(\text{clear-sky})}^{in} \Psi_{Transmission},$$

and using a fit to within 0.05 of the Ψ functions from Figure 3 of Stephens (1978) for transmission/absorption of short-wave radiation (ignoring zenith angle dependence)

$$\Psi_{Transmission} = \begin{cases} \exp(-16W^{in} + 13W^{in^2}), & W^{in} \leq 0.11 \\ 0.2; & W^{in} > 0.11 \end{cases},$$

$$\Psi_{Absorption} = \begin{cases} 0.3W^{in^{1/2}}; & W^{in} \leq 0.11 \\ 0.1; & W^{in} > 0.11 \end{cases}.$$

The incoming long-wave radiation is

$$R_{lw}^{in}(\sigma) = R_{lw(clear-sky)}^{in} (1 - \varepsilon_{lw}^{in}(\sigma)) + \varepsilon_{lw}^{in}(\sigma) \sigma_{SB} T^4(\sigma),$$

$$\varepsilon_{lw}^{in}(\sigma) = \min(0.9, 1 - \exp(-158W^{in}))$$

with the incoming liquid water path

$$W^{in} = \int_{\sigma}^{z_T} \rho_a \min(0.0003, q_C) d\sigma.$$

Radiative heating and cooling at each model level is accounted for via the source term in the prognostic equation for temperature with

$$\frac{\partial T}{\partial t} \Big|_{RADIATION} = \frac{\partial T}{\partial t} \Big|_{RADIATION(clear-sky)} + \frac{1}{\rho c_p} \frac{\partial \Psi_{Heat}}{\partial \sigma} \frac{\partial \sigma}{\partial z},$$

where

$$\Psi_{Heat}(\sigma) = R_{sw(clear-sky)}^{in} \Psi_{Absorption} + R_{lw}^{in}(\sigma) - R_{lw}^{out}(\sigma),$$

with the incoming short-wave and long-wave components from the above expressions, and the outgoing long-wave radiation from

$$R_{lw}^{out}(\sigma) = R_{lw(clear-sky)}^{out} (1 - \varepsilon_{lw}^{out}(\sigma)) + \varepsilon_{lw}^{out}(\sigma) \sigma_{SB} T^4(\sigma),$$

$$\varepsilon_{lw}^{out}(\sigma) = \min(0.9, 1 - \exp(-130W^{out}))$$

with the outgoing liquid water path

$$W^{out} = \int_{z_S}^{\sigma} \rho_a \min(0.0003, q_C) d\sigma.$$

2.6 Surface boundary conditions

Boundary conditions for mean variables at the surface are zero velocity, π_0 from the hydrostatic equation (5), $\theta_{v0} = c_p T_0 (1 + 0.61 q_0) / \pi_0$, with $T_0 = (1 - \sigma_f) T_g + \sigma_f T_f$ and $q_0 = (1 - \sigma_f) q_g + \sigma_f q_f$, where σ_f is the fraction of foliage cover and subscripts g and f denote soil and foliage respectively. The soil and vegetation parameterisations described below are based on those from Kowalczyk *et al.* (1991).

Note that if the surface type is water, then the surface temperature is set equal to the water surface temperature, and surface moisture is set equal to the saturation value. If the surface type is permanent ice/snow, then the surface temperature is set equal to -4°C , and surface moisture is set equal to the saturation value.

2.6.1 Soil parameterisation

Equations for soil temperature T_g , moisture content η_g and specific humidity q_g are

$$\frac{\partial T_g}{\partial t} = \frac{3.72 G_g}{\rho_s c_s d'_1} - \frac{7.4(T_g - T_d)}{24 \times 3600},$$

$$\frac{\partial \eta_g}{\partial t} = -\frac{c_1 (E_g (1 - \sigma_f) - \rho_w ((1 - \sigma_f) P + \sigma_f P_g - R))}{\rho_w d_1} - \frac{c_2 (\eta_g - \eta_{eq})}{24 \times 3600},$$

$$q_g = f_{wet} q_0^* + (1 - f_{wet}) q_1,$$

where

$$G_g = R_{sw}^{in} (1 - \alpha_g) + R_{lw}^{in} - \sigma_{SB} T_g^4 \cos \alpha - H_g - \lambda E_g = \text{soil heat flux (W m}^{-2}\text{)},$$

$$H_g = \rho c_p (\theta_g - \theta_1) / r_H = \text{sensible heat flux (W m}^{-2}\text{)},$$

$$\lambda E_g = \rho \lambda (q_g - q_1) / r_H = \text{evaporative heat flux (W m}^{-2}\text{)},$$

r_H is the aerodynamic resistance (see Section 2.6.4) with a roughness length of 0.05 m,

$$\eta_{eq} = \eta_d - \eta_{sat} a_\eta \left(\frac{\eta_d}{\eta_{sat}} \right)^{b_\eta} \left(1 - \left(\frac{\eta_d}{\eta_{sat}} \right)^{8b_\eta} \right),$$

T_d, η_d = deep soil temperature and moisture (model input),

$$\lambda = 2.5 \times 10^6 \text{ J kg}^{-1}, \rho_w = 1000 \text{ kg m}^{-3},$$

$$d'_1 = \sqrt{\frac{k_s \times 24 \times 3600}{\rho_s c_s \pi_c}}, \quad d_1 = 0.1,$$

$\alpha_g, k_s, \rho_s, c_s$ = soil albedo, conductivity, density, and heat capacity,

P, P_g = precipitation reaching the vegetation and soil respectively,

q_g^* = soil saturated specific humidity,

R = runoff.

The soil characteristics are specified for three soil types

$$k_s = 419(a_s \eta_g - b_s \eta_g^{0.4}),$$

$$\rho_s c_s = (1 - \eta_{sat}) \rho_s^{dry} c_s^{dry} + \eta_g \rho_w c_w,$$

$$c_w = 4186,$$

Sand :

$$c_1 = \begin{cases} 10 & ; \text{for } \eta_r \leq 0.05, \\ \frac{(1.8\eta_r + 0.962)}{(5.0\eta_r + 0.2)} & ; \text{otherwise.} \end{cases}$$

$$c_2 = 2.0;$$

$$f_{wet} = \begin{cases} 1 & ; \text{for } \eta_r \geq 0.15, \\ 11.49(\eta_r - 0.063) & ; \text{for } 0.063 \leq \eta_r \leq 0.15, \\ 0 & ; \text{for } \eta_r < 0.063. \end{cases}$$

$$\eta_r = \eta_0 / \eta_{sat}, \eta_{sat} = 0.395, \eta_{wilt} = 0.068,$$

$$a_s = 0.004, b_s = 0.006, \rho_s^{dry} = 1600, c_s^{dry} = 800, a_\eta = 0.387, b_\eta = 4.$$

Sandy Clay Loam :

$$c_1 = \begin{cases} 10 & ; \text{for } \eta_r \leq 0.226, \\ \frac{(1.78\eta_r + 0.253)}{(2.96\eta_r - 0.581)} & ; \text{otherwise.} \end{cases}$$

$$c_2 = 3.0;$$

$$f_{wet} = \begin{cases} 1 & ; \text{for } \eta_r \geq 0.365, \\ 6.90(\eta_r - 0.22) & ; \text{for } 0.22 \leq \eta_r \leq 0.365, \\ 0 & ; \text{for } \eta_r < 0.22. \end{cases}$$

$$\eta_r = \eta_0 / \eta_{sat}, \eta_{sat} = 0.420, \eta_{wilt} = 0.175,$$

$$a_s = 0.003, b_s = 0.004, \rho_s^{dry} = 1600, c_s^{dry} = 845, a_\eta = 0.135, b_\eta = 6.$$

Clay :

$$c_1 = \begin{cases} 10 & ; \text{for } \eta_r \leq 0.421, \\ \frac{(2.22\eta_r - 0.556)}{(2.78\eta_r - 1.114)} & ; \text{otherwise.} \end{cases}$$

$$c_2 = 1.9;$$

$$f_{wet} = \begin{cases} 1 & ; \text{for } \eta_r \geq 0.52, \\ 8.33(\eta_r - 0.40) & ; \text{for } 0.40 \leq \eta_r \leq 0.52, \\ 0 & ; \text{for } \eta_r < 0.40. \end{cases}$$

$$\eta_r = \eta_0 / \eta_{sat}, \eta_{sat} = 0.482, \eta_{wilt} = 0.286,$$

$$a_s = 0.002, b_s = 0.003, \rho_s^{dry} = 1600, c_s^{dry} = 890, a_\eta = 0.083, b_\eta = 12.$$

2.6.2 Vegetation parameterisation

The vegetation temperature T_f is calculated from a surface energy balance

$$0 = R_{sw}^{in} (1 - \alpha_f) + R_{lw}^{in} - \sigma_{SB} T_f^4 \cos \alpha - H_f - \lambda E_f$$

using Newton iteration, where the outward long-wave radiation and sensible (H_f) and latent (E_f) heat fluxes are treated as functions of T_f , with

$$H_f = \rho c_p (\theta_f - \theta_1) / r_H,$$

$$E_f = (1 - \beta) E_{tr} + \beta E_w,$$

$$E_{tr} = \rho (q_f^* - q_1) / (r_H + r_s),$$

$$E_w = \rho (q_f^* - q_1) / r_H,$$

$$\beta = \begin{cases} 1; & \text{if condensation } (q_1 > q_f^*) \\ m_r / (0.0002 LAI); & \text{if evapotranspiration} \end{cases}$$

$$\frac{\partial m_r}{\partial t} = P - P_g - \beta E_w / \rho_w,$$

where m_r is the moisture reservoir and r_H is the aerodynamic resistance (see Section 2.6.4).

Table 1: Vegetation (land-use) characteristics used in TAPM.

Vegetation Types:	h_f (m)	σ_f	LAI	r_{si} (m ⁻¹)
-1: Permanent snow/ice	-	-	-	-
0: Water	-	-	-	-
1: Forest – tall dense	42.00	0.75	4.8	370
2: Forest – tall mid-dense	36.50	0.75	6.3	330
3: Forest – dense	25.00	0.75	5.0	260
4: Forest – mid-dense	17.00	0.50	3.8	200
5: Forest – sparse (woodland)	12.00	0.25	2.8	150
6: Forest – very sparse (woodland)	10.00	0.25	2.5	130
7: Forest – low dense	9.00	0.75	3.9	200
8: Forest – low mid-dense	7.00	0.50	2.8	150
9: Forest – low sparse (woodland)	5.50	0.25	2.0	110
10: Shrub-land – tall mid-dense (scrub)	3.00	0.50	2.6	160
11: Shrub-land – tall sparse	2.50	0.25	1.7	100
12: Shrub-land – tall very sparse	2.00	0.25	1.9	120
13: Shrub-land – low mid-dense	1.00	0.50	1.4	90
14: Shrub-land – low sparse	0.60	0.25	1.5	90
15: Shrub-land – low very sparse	0.50	0.25	1.2	80
16: Grassland – sparse hummock	0.50	0.25	1.6	90
17: Grassland – very sparse hummock	0.45	0.25	1.4	90
18: Grassland – dense tussock	0.75	0.75	2.3	150
19: Grassland – mid-dense tussock	0.60	0.50	1.2	80
20: Grassland – sparse tussock	0.45	0.25	1.7	100
21: Grassland – very sparse tussock	0.40	0.25	1.2	80
22: Pasture/herb-field – dense (perennial)	0.60	0.75	2.3	80
23: Pasture/herb-field – dense (seasonal)	0.60	0.75	2.3	80
24: Pasture/herb-field – mid-dense (perennial)	0.45	0.50	1.2	40
25: Pasture/herb-field – mid-dense (seasonal)	0.45	0.50	1.2	40
26: Pasture/herb-field – sparse	0.35	0.25	1.9	120
27: Pasture/herb-field – very sparse	0.30	0.25	1.0	80
28: Littoral	2.50	0.50	3.0	180
29: Permanent lake	-	-	-	-
30: Ephemeral lake (salt)	-	-	-	-
31: Urban	10.00	0.75	2.0	100

The vegetation specific humidity q_f is calculated from $q_f = q_f^* - E_f r_s / \rho$, and the stomatal resistance r_s is calculated using

$$r_s = \frac{r_{si}}{LAI} F_1 F_2^{-1} F_3^{-1} F_4^{-1}$$

and

$$F_1 = \frac{1+f}{f+(r_{si}/5000)}, \quad F_2 = \frac{\eta_d - \eta_{wilt}}{0.75\eta_{sat} - \eta_{wilt}},$$

$$F_3 = 1 - 0.00025(e_f^* - e_1), \quad F_4 = 1 - 0.0016(298 - T_1)^2, \quad f = 0.55 \frac{R_{sw}^{in}}{R^*} \frac{2}{LAI}.$$

Other variables are

α_f = Vegetation albedo (0.2),

q_f^* = Vegetation saturated specific humidity,

e_f^* = Vegetation saturated vapour pressure,

$$R^* = \begin{cases} 30 \text{ W m}^{-2}; & \text{if } z_{0f} > 0.3 \\ 100 \text{ W m}^{-2}; & \text{if } z_{0f} \leq 0.3 \end{cases}$$

z_{0f} = Vegetation roughness length (m) = $h_f / 10$ ($0.05 \leq z_{0f} \leq 1.00$ m),

h_f = Vegetation height (m),

σ_f = Fraction of surface covered by vegetation,

LAI = Leaf Area Index,

r_{si} = minimum stomatal resistance (s^{-1}).

The vegetation (land-use) types used in TAPM are based on a CSIRO Wildlife and Ecology Categorisation (Graetz, 1998, personal communication), and are listed in Table 1, with urban conditions modified as described in Section 2.6.3.

2.6.3 Urban Parameterisation

The single urban category can be thought of as medium density urban conditions. Central city land-use is approximated by this category, and so parameter values for roughness, urban fraction, and anthropogenic heat flux may be underestimated. Suburban land-use is approximated by rural conditions in TAPM.

In urban regions the surface temperature and specific humidity are calculated using $T_0 = (1 - \sigma_U)T_{g\&f} + \sigma_U T_U$ and $q_0 = (1 - \sigma_U)q_{g\&f} + \sigma_U q_U$, where $\sigma_U = 0.5$ is the fraction of urban cover, and subscript U denotes urban and $g\&f$ denotes the combined soil and foliage values respectively.

The equations for urban temperature T_U and specific humidity q_U use a similar approach as that for soil temperature, except that the surface properties are those of urban surfaces such as concrete/asphalt/roofs:

$$\frac{\partial T_U}{\partial t} = \frac{3.72G_U}{\rho_U c_U d_U} - \frac{7.4(T_U - T_d)}{24 \times 3600},$$

$$q_U = 0,$$

where

$$G_U = R_{sw}^{in}(1 - \alpha_U) + R_{lw}^{in} - \varepsilon_U \sigma_{SB} T_U^4 \cos \alpha - H_U - \lambda E_U + A_U$$

= urban surface heat flux (W m^{-2}),

$$H_U = \rho c_p (\theta_U - \theta_1) / r_H = \text{urban sensible heat flux (W m}^{-2}\text{)},$$

$$\lambda E_U = 0 = \text{urban evaporative heat flux (W m}^{-2}\text{)},$$

$$d_U = \sqrt{\frac{k_U \times 24 \times 3600}{\rho_U c_U \pi_c}},$$

and the urban surface albedo (α_U), emissivity (ε_U) and anthropogenic heat flux (A_U) from Oke (1988) are $\alpha_U = 0.15$, $\varepsilon_U = 0.95$ and $A_U = 30 \text{ W m}^{-2}$. The urban surface thermal conductivity (k_U), density (ρ_U) and specific heat capacity (c_U), from Pielke (1984), are $k_U = 4.6 \text{ W m}^{-1} \text{ K}^{-1}$, $\rho_U = 2300 \text{ kg m}^{-3}$, $c_U = 879 \text{ J kg}^{-1} \text{ K}^{-1}$ (based on the characteristics of concrete).

Urban surface layer scaling variables are calculated using the same approach as for soil and vegetation, with an urban roughness length of 1 m.

Note that the anthropogenic heat flux (A_U) is also included in the soil and vegetation surface flux equations when the land-use category is urban.

2.6.4 Surface fluxes and turbulence

Boundary conditions for the turbulent fluxes are determined by Monin-Obukhov surface layer scaling variables with stability functions from Dyer and Hicks (1970)

$$\overline{w'u'}|_0 = -u_*^2 u / \sqrt{u_1^2 + v_1^2}, \quad \overline{w'v'}|_0 = -u_*^2 v / \sqrt{u_1^2 + v_1^2}, \quad \overline{w'\theta_v'}|_0 = -u_* \theta_{v*}, \quad \overline{w'q'}|_0 = -u_* q_*,$$

where

$$u_* = k \sqrt{u_1^2 + v_1^2} / I_M, \quad \theta_{v*} = k(\theta_{v1} - \theta_{v0}) / I_H, \quad \theta_* = k(\theta_1 - \theta_0) / I_H, \quad q_* = k(q_1 - q_0) / I_H,$$

$$I_M = \begin{cases} \ln\left(\frac{z_1}{z_0}\right) - 2 \ln\left(\frac{1 + \phi_M^{-1}(z_1)}{1 + \phi_M^{-1}(z_0)}\right) - \ln\left(\frac{1 + \phi_M^{-2}(z_1)}{1 + \phi_M^{-2}(z_0)}\right) \\ \quad + 2(\tan^{-1}(\phi_M^{-1}(z_1)) - \tan^{-1}(\phi_M^{-1}(z_0))) \text{ if } \frac{z_1}{L} < 0, \\ \ln\left(\frac{z_1}{z_0}\right) + 5\left(\frac{z_1 - z_0}{L}\right) \text{ if } \frac{z_1}{L} \geq 0 \end{cases}$$

$$I_H = I_{aH} + I_{bH},$$

$$I_{aH} = \begin{cases} \ln\left(\frac{z_1}{z_0}\right) - 2 \ln\left(\frac{1 + \phi_H^{-1}(z_1)}{1 + \phi_H^{-1}(z_T)}\right) \text{ if } \frac{z_1}{L} < 0 \\ \ln\left(\frac{z_1}{z_0}\right) + 5\left(\frac{z_1 - z_T}{L}\right) \text{ if } \frac{z_1}{L} \geq 0 \end{cases},$$

$$I_{bH} = \ln\left(\frac{z_0}{z_T}\right)$$

$$r_H = I_H / (k u_*), \quad r_{aH} = I_{aH} / (k u_*), \quad r_{bH} = I_{bH} / (k u_*),$$

$$\phi_M = \begin{cases} \left(1 - 16 \frac{z}{L}\right)^{-1/4}; & \text{for } \frac{z}{L} < 0 \\ \left(1 + 5 \frac{z}{L}\right); & \text{for } \frac{z}{L} \geq 0 \end{cases}, \quad \phi_H = \begin{cases} \left(1 - 16 \frac{z}{L}\right)^{-1/2}; & \text{for } \frac{z}{L} < 0 \\ \left(1 + 5 \frac{z}{L}\right); & \text{for } \frac{z}{L} \geq 0 \end{cases},$$

with $\frac{z}{L} = \frac{kzg\theta_{v^*}}{u_*^2\theta_v}$, and $z_T = z_0/7.4$ from Garratt (1992),

and the gradient Richardson number $R_{ig} = \frac{z}{L} \frac{\phi_H}{\phi_M^2}$,

which in the stable limit gives a critical value of $R_{igc} = 0.2$.

These equations are solved iteratively, with the restrictions that $\sqrt{u_1^2 + v_1^2} \geq 0.5 \text{ m s}^{-1}$, $z_1 / L \leq 1$, and $0.05 \leq u_* \leq 1.0 \text{ m s}^{-1}$.

Turbulence boundary conditions are specified at the first model level using surface and mixed layer scaling, for the prognostic turbulence equations

$$E = c_m^{-1/2} u_*^2 + 0.5 w_*^2 \quad \text{and} \quad \varepsilon = \frac{u_*^3}{kz} \phi_m - \frac{g}{\theta_v} u_* \theta_{v^*},$$

where w_* is the convective velocity scale (m s^{-1}) defined as

$$w_* = \left(\frac{-gz_i u_* \theta_{v^*}}{\theta_v} \right)^{1/3},$$

and z_i is the convective boundary-layer height (m). The boundary-layer height in convective conditions is defined as the first model level above the surface for which the vertical heat flux is negative, while in stable/neutral conditions it is defined as the first model level above the surface that has a vertical heat flux less than 5% of the surface value following Derbyshire (1990).

2.7 Initial conditions and boundary conditions

The model is initialised at each grid point with values of $u_s, v_s, \theta_{vs}, q_s$ interpolated from the synoptic analyses. Iso-lines of these variables are oriented to be parallel to mean sea level (i.e. cutting into the terrain). Turbulence levels are set to their minimum values as the model is started at midnight. The Exner pressure function is integrated from mean sea level to the model top to determine the top boundary condition. The Exner pressure and terrain-following vertical velocity are then diagnosed using equations (3) and (5) respectively. Surface temperature and moisture are set to the deep soil values specified, with surface temperature adjusted for terrain height using the synoptic lapse rate. At the model top boundary, all variables are set at their synoptic values.

One-way nested lateral boundary conditions are used for the prognostic equations (1), (2), (4), and (7) using an approach based on Davies (1976). For example for u , an additional term is added to the right hand side of equation (1).

$$\frac{du}{dt} = RHS(u) - F_{NEST} \frac{(u - \tilde{u})}{3\Delta t}$$

where \tilde{u} is interpolated from the coarse outer grid onto the fine inner grid, and

$$F_{NEST} = \max(G_x, G_y)$$

$$G_x = \begin{cases} 1 - \left(\frac{i-1}{n_b} \right)^2; & \text{for } i = 1, \dots, n_b; \\ 1 - \left(\frac{n_x - i}{n_b} \right)^2; & \text{for } i = n_x - (n_b - 1), \dots, n_x; \\ 0; & \text{otherwise.} \end{cases}$$

and similarly for G_y , with n_x the number of grid points in the x direction, and $n_b = 5$ the number of grid points in from the grid edge over which the solutions are meshed. On the outer grid, this same nesting procedure is used, but using time-interpolated synoptic winds, temperature and moisture. Note that the terrain is smoothed near the lateral boundaries to reduce noise created by the boundary conditions.

2.8 Assimilation of wind observations

The method used to optionally assimilate wind observations is based on the approach of Stauffer and Seaman (1994), where a nudging term is added to the horizontal momentum equations (for u and v). The equation for u is

$$\frac{\partial u}{\partial t} = RHS(u) + G \left(\frac{\sum_{n=1}^{nsite} W_n (u_n - \hat{u}_n)}{\sum_{n=1}^{nsite} W_n} \right),$$

where

G = nudging coefficient = $1/(3\Delta t)$,

Δt = model meteorological advection timestep,

u_n = observed u at observation site n ,

\hat{u}_n = model u interpolated to observation site n ,

$$W_n = \begin{cases} Q_n \left(\frac{R_n^2 - D_n^2}{R_n^2 + D_n^2} \right); & \text{if } D_n < R_n; \\ 0; & \text{otherwise.} \end{cases}$$

Q_n = data quality indicator [0...1],

R_n = radius of influence (m),

$$D_n^2 = (x_i - x_n)^2 + (y_j - y_n)^2,$$

(x_i, y_j) = location of grid point,

(x_n, y_n) = location of observation site.

Note that observations at any height can be included, and the observations can influence a user-specified number of model levels for each site.

3 Air pollution component

3.1 Eulerian grid module

The Eulerian Grid Module (EGM) consists of nested grid-based solutions of the Eulerian concentration equation representing advection, diffusion, and chemical reactions. Dry and wet deposition processes are also included.

3.1.1 Pollutant equations

The prognostic equation for concentration χ is similar to that for the potential virtual temperature and specific humidity variables, and includes advection, diffusion, and terms to represent pollutant emissions S_χ and chemical reactions R_χ

$$\frac{d\chi}{dt} = \frac{\partial}{\partial x} \left(K_\chi \frac{\partial \chi}{\partial x} \right) + \frac{\partial}{\partial y} \left(K_\chi \frac{\partial \chi}{\partial y} \right) - \left(\frac{\partial \sigma}{\partial z} \right) \frac{\partial}{\partial \sigma} \left(\overline{w' \chi'} \right) + S_\chi + R_\chi. \quad (11)$$

The expression for the vertical flux of tracer concentration includes counter-gradient fluxes as follows

$$\overline{w' \chi'} = -K_\chi \frac{\partial \chi}{\partial \sigma} \frac{\partial \sigma}{\partial z} + \frac{(1 - c_{\chi^3})}{c_{\chi^1}} \frac{E}{\varepsilon} \frac{g}{\theta_v} \overline{\theta'_v \chi'}$$

with

$$\begin{aligned} \frac{d\overline{\theta'_v \chi'}}{dt} = & \frac{\partial}{\partial x} \left(K_\chi \frac{\partial \overline{\theta'_v \chi'}}{\partial x} \right) + \frac{\partial}{\partial y} \left(K_\chi \frac{\partial \overline{\theta'_v \chi'}}{\partial y} \right) + \left(\frac{\partial \sigma}{\partial z} \right)^2 \frac{\partial}{\partial \sigma} \left(K_\chi \frac{\partial \overline{\theta'_v \chi'}}{\partial \sigma} \right) \\ & + (K + K_\chi) \left(\left(\frac{\partial \theta_v}{\partial x} + \frac{\partial \theta_v}{\partial \sigma} \frac{\partial \sigma}{\partial x} \right) \left(\frac{\partial \chi}{\partial x} + \frac{\partial \chi}{\partial \sigma} \frac{\partial \sigma}{\partial x} \right) + \left(\frac{\partial \theta_v}{\partial y} + \frac{\partial \theta_v}{\partial \sigma} \frac{\partial \sigma}{\partial y} \right) \left(\frac{\partial \chi}{\partial y} + \frac{\partial \chi}{\partial \sigma} \frac{\partial \sigma}{\partial y} \right) \right) \\ & - \overline{w' \theta'_v} \frac{\partial \chi}{\partial \sigma} \frac{\partial \sigma}{\partial z} - \overline{w' \chi'} \frac{\partial \theta_v}{\partial \sigma} \frac{\partial \sigma}{\partial z} - \frac{2}{c_\chi} \frac{\varepsilon}{E} \overline{\theta'_v \chi'}. \end{aligned} \quad (12)$$

Constants in these equations are $c_{\chi^1} = 3.0$, $c_{\chi^3} = 0.5$, and $c_\chi = 1.6$, based on those used by Rodi (1985). The form of these equations has been used in many of the second order closure models for a meteorological scalar, and has been used by Enger (1986) for dispersion in a convective boundary layer, although he also used a prognostic equation for $\overline{w' \chi'}$. The diffusion coefficient used for pollutant concentration is $K_\chi = 2.5K$, consistent with meteorological variables (see Section 2.4).

Initially χ is set to a background concentration. Values of $\overline{\theta'_v \chi'}$ are initialised to zero as conditions are thermally stable, and if counter-gradient fluxes are assumed unimportant for a particular simulation, the solution of equation (12) is omitted and $\overline{\theta'_v \chi'}$ is set to zero. Generally, counter-gradient fluxes are only important for near-source diffusion of point sources, and only when the model resolution is fine enough (less than 1 km) to resolve near-source concentrations adequately.

For pollutant concentration at inflow boundaries on the outermost grid, a background concentration is specified, while values at the boundaries of inner grids are obtained from the previous nest. At outflow boundaries, zero gradient boundary conditions are used. Zero gradient boundary conditions are used for $\overline{\theta'_v \chi'}$ on all grids.

3.1.2 Chemistry

The model can be run in either tracer mode or in chemistry mode. In tracer mode, the only chemical reaction is an optional exponential decay $R_\chi = -k_{decay}\chi$, where the decay rate k_{decay} is a model input. In chemistry mode, gas-phase photochemistry is based on the semi-empirical mechanism called the Generic Reaction Set (GRS) of Azzi *et al.* (1992), with the hydrogen peroxide modification of Venkatram *et al.* (1997). We have also included gas- and aqueous-phase reactions of sulfur dioxide and particles, with the aqueous-phase reactions based on Seinfeld and Pandis (1998).

In chemistry mode, there are ten reactions for thirteen species: smog reactivity (R_{smog}), the radical pool (RP), hydrogen peroxide (H_2O_2), nitric oxide (NO), nitrogen dioxide (NO_2), ozone (O_3), sulfur dioxide (SO_2), stable non-gaseous organic carbon (SNGOC), stable gaseous nitrogen products (SGN), stable non-gaseous nitrogen products (SNGN), stable non-gaseous sulfur products (SNGS), plus Airborne Particulate Matter (APM) and Fine Particulate Matter (FPM) that include secondary particulate concentrations consisting of (SNGOC), (SNGN), and (SNGS).

The reactions are

Reactions	Reaction Rates
$R_{smog} + h\nu \rightarrow RP + R_{smog} + \eta SNGOC$	$R_1 = k_1[R_{smog}]$
$RP + NO \rightarrow NO_2$	$R_2 = k_2[RP][NO]$
$NO_2 + h\nu \rightarrow NO + O_3$	$R_3 = k_3[NO_2]$
$NO + O_3 \rightarrow NO_2$	$R_4 = k_4[NO][O_3]$
$RP + RP \rightarrow RP + \alpha H_2O_2$	$R_5 = k_5[RP][RP]$
$RP + NO_2 \rightarrow SGN$	$R_6 = k_6[RP][NO_2]$
$RP + NO_2 \rightarrow SNGN$	$R_7 = k_7[RP][NO_2]$
$RP + SO_2 \rightarrow SNGS$	$R_8 = k_8[RP][SO_2]$
$H_2O_2 + SO_2 \rightarrow SNGS$	$R_9 = k_9[H_2O_2][SO_2]$
$O_3 + SO_2 \rightarrow SNGS$	$R_{10} = k_{10}[O_3][SO_2]$

where $[A]$ denotes concentration of species A and $h\nu$ denotes photo-synthetically active radiation.

Yield coefficients are

$$\alpha = \max\left(0.03, \exp\left(-0.0261 \frac{[R_{smog}]}{[NO_x]}\right)\right),$$

$$\eta = 0.1,$$

and reaction rate coefficients are

$$k_1 = k_3 f,$$

$$k_2 = 3580/(60T),$$

$$k_3 = 0.0001\delta.TSR/60,$$

$$k_4 = (924/60T)\exp(-1450/T),$$

$$k_5 = (10/60),$$

$$k_6 = (0.12/60),$$

$$k_7 = k_6,$$

$$k_8 = (0.003/60),$$

$$k_9 = \frac{7.45 \times 10^7 [H^+] \alpha_1}{1 + 13[H^+]} K_{H-S(IV)} K_{H-H_2O_2} L \cdot R \cdot T \cdot 10^{-9},$$

$$k_{10} = (2.4 \times 10^4 \alpha_0 + 3.7 \times 10^5 \alpha_1 + 1.5 \times 10^9 \alpha_2) K_{H-S(IV)} K_{H-O_3} L \cdot R \cdot T \cdot 10^{-9},$$

with

$$[H^+] = 10^{-pH},$$

$$\alpha_0 = \frac{K_{H0-SO_2}}{K_{H-S(IV)}}, \alpha_1 = \alpha_0 \frac{K_{H1-SO_2}}{[H^+]}, \alpha_2 = \alpha_1 \frac{K_{H2-SO_2}}{[H^+]},$$

$$K_{H-S(IV)} = K_{H0-SO_2} \left(1 + \frac{K_{H1-SO_2}}{[H^+]} \left(1 + \frac{K_{H2-SO_2}}{[H^+]} \right) \right),$$

$$K_{H0-SO_2} = 1.24 \exp \left(-3120 \left(\frac{1}{298} - \frac{1}{T} \right) \right)$$

$$K_{H1-SO_2} = 1.29 \times 10^{-2} \exp \left(-2080 \left(\frac{1}{298} - \frac{1}{T} \right) \right)$$

$$K_{H2-SO_2} = 6.014 \times 10^{-8} \exp \left(-1120 \left(\frac{1}{298} - \frac{1}{T} \right) \right)$$

$$K_{H-H_2O_2} = 7.1 \times 10^4 \exp \left(-7250 \left(\frac{1}{298} - \frac{1}{T} \right) \right)$$

$$K_{H-O_3} = 9.4 \times 10^{-3} \exp \left(-2520 \left(\frac{1}{298} - \frac{1}{T} \right) \right)$$

$$(\text{all } K_H \leq (L \cdot R \cdot T)^{-1}),$$

where APM and FPM are in $\mu\text{g m}^{-3}$, all other species are in units of ppb, the rate coefficients k_1, k_3 are in s^{-1} and $k_2, k_4, k_5, k_6, k_7, k_8, k_9, k_{10}$ are in $\text{ppb}^{-1} \text{s}^{-1}$, temperature T is in K, the total solar radiation TSR is in W m^{-2} , R is the gas constant (0.082) in $\text{atm M}^{-1} \text{K}^{-1}$, L is the volume based liquid water fraction related to the liquid water specific humidity by $L = q_L \rho / \rho_w$,

$$f = \exp \left(-4700 \left(\frac{1}{T} - \frac{1}{316} \right) \right),$$

$$\delta = \begin{cases} 4.23 + 1.09 / \cos Z; & \text{if } 0 \leq Z \leq 47 \\ 5.82; & \text{if } 47 \leq Z \leq 64, \\ -0.997 + 12(1 - \cos Z); & \text{if } 64 \leq Z \leq 90 \end{cases}$$

and Z is the zenith angle in degrees.

The yield factor η , the reaction rate k_8 , and the secondary formation of APM and FPM by the various processes, are in a preliminary form that needs to be verified against appropriate data.

The concept of using R_{smog} rather than Volatile Organic Compounds (VOCs) in the reaction equations follows from the work of Johnson (1984). The concentration of R_{smog} is defined as a reactivity coefficient multiplied by VOC concentration. For example, Johnson (1984) used $[R_{smog}] = 0.0067[\text{VOC}]$ for typical 1980s Australian urban air dominated by motor vehicles. Empirically determined reactivity coefficients for individual VOC species are available from smog chamber experiments, while numerically determined reactivity coefficients have been calculated by comparison of the GRS mechanism with more complex mechanisms (M. Cope, 1999, personal communication)

Emissions from VOC sources usually consist of more than one type of VOC, necessitating the R_{smog} emission rate to be calculated in the following way

$$Q_{Rsmog} = \sum_i \frac{14CN_i}{MW_i} a_i Q_i ,$$

where Q_i is the emission rate (g s^{-1}) for each VOC, a_i is its reactivity, CN_i is its carbon number and MW_i is its molecular weight. An alternative (and more precise) approach is to use a standard reactivity coefficient for a standard VOC mixture (for example $Q_{Rsmog} = 0.0064Q_{VOC}$) with perturbations about this standard accounted for using the individual species reactivity coefficients (M. Cope, 1999, personal communication). Sample perturbation coefficients for the Carbon Bond IV (CBIV) mechanism are summarised in Table 2.

Table 2 : Characteristics of the CBIV lumped VOC species needed for the GRS mechanism (Cope, 1999, personal communication).

CBIV Lumped VOC Species (i)	Carbon Number (CN_i)	Molecular Weight (MW_i)	CBIV Reactivity (a_i) (ppb ppbC $^{-1}$)
Formaldehyde (FORM) (CH_2O)	1	30	0.0174
Higher Aldehydes (ALD2) ($\text{C}_2\text{H}_4\text{O}$)	2	44	-0.00081
Ethene (ETH) (C_2H_4)	2	28	0.0153
Alkenes (Olefins) (OLE) (C_2H_4)	2	28	0.0127
Alkanes (Paraffins) (PAR) (CH_2)	1	14	0.00095
Toluene (TOL) (C_7H_8)	7	92	0.0049
Xylene (XYL) (C_8H_{10})	8	106	0.0145
Isoprene (ISOP) (C_5H_8)	5	68	0.0092

If we define $[NO_x] = [NO] + [NO_2]$ and $[SP_x] = [O_3] + [NO_2]$ (analogous to the definition of smog produced by Johnson, 1984, but without including SGN and SNGN), we do not need the differential equations for NO and O_3 . The resulting reaction terms for the prognostic equation (11) for the nine pollutants APM, FPM, SO_2 , NO_x , R_{smog} , SP_x , NO_2 , RP, and H_2O_2 are

$$R_{[APM]} = F_{\text{CH}_2}\eta R_1 + F_{\text{HNO}_3}R_7 + F_{\text{H}_2\text{SO}_4}(R_8 + R_9 + R_{10})$$

$$R_{[FPM]} = F_{\text{CH}_2}\eta R_1 + 0.5F_{\text{HNO}_3}R_7 + F_{\text{H}_2\text{SO}_4}(R_8 + R_9 + R_{10})$$

$$R_{[\text{SO}_2]} = -R_8 - R_9 - R_{10}$$

$$R_{[NO_x]} = -R_6 - R_7$$

$$R_{[R_{smog}]} = 0$$

$$R_{[SP_x]} = R_2 - R_6 - R_7 - R_{10}$$

$$R_{[NO_2]} = R_2 - R_3 + R_4 - R_6 - R_7$$

$$R_{[RP]} = R_1 - R_2 - R_5 - R_6 - R_7 - R_8$$

$$R_{[H_2O_2]} = \alpha R_5 - R_9$$

where $F_{HNO_3} = 2.6$, $F_{H_2SO_4} = 4.0$, $F_{CH_2} = 0.57$, are approximate factors to convert the stable non-gaseous compounds to APM in $\mu\text{g m}^{-3}$ at NTP.

The potentially fast reactions in the reduced system are for SO_2 , NO_2 , RP, and H_2O_2 . This implies that a small explicit timestep is necessary, but this restriction can be overcome by using a simple implicit solution procedure described later. This approach then allows large numerical time-steps to be used, provided the pH of the liquid water present is below about 5.5 (so that the reaction between O_3 and SO_2 to produce SNGS (R_{10}) does not dominate the aqueous phase reactions). Note that the default pH of the liquid water present in the model is 4.5, which is typical of Australian conditions.

3.1.3 Deposition

The dry deposition formulation for gaseous pollutants follows that of Physick (1994) in which all scalars behave like heat in terms of roughness length and stability function. Knowing the resistance functions for heat transfer r_{aH} and r_{bH} (Section 2.6.4), and the stomatal resistance r_s (Section 2.6.2), the surface flux for variable χ is written as $\overline{w'\chi'}|_o = -\chi_1 V_d$, where the pollutant deposition velocity is $V_d = (r_{aero} + r_{surface})^{-1}$, the aerodynamic resistance is $r_{aero} = r_{aH} + r_{bH} Sc^{2/3}$, the surface resistance $r_{surface}$ depends on the surface type, and Sc is the Schmidt Number (the ratio of the molecular diffusivities for water vapour and pollutant concentration).

$$\text{For a land surface, } V_d = \frac{\sigma_f \beta}{r_{aero} + r_{water}} + \frac{\sigma_f (1 - \beta)}{r_{aero} + r_s Sc} + \frac{(1 - \sigma_f)}{r_{aero} + r_{soil}}$$

$$\text{and for a water surface, } V_d = \frac{1}{r_{aero} + r_{water}}.$$

Non-zero deposition velocities are used for the gaseous pollutants NO_2 , NO , O_3 , SO_2 and H_2O_2 , with resistance values based on information in Wesley (1989) and Harley *et al.* (1993)

$$\text{NO}_2: \quad r_{water} = 1000, r_{soil} = 1000, Sc = \sqrt{46/18};$$

$$\text{NO:} \quad r_{water} = 10000, r_{soil} = 10000, Sc = \sqrt{30/18};$$

$$\text{O}_3: \quad r_{water} = 2000, r_{soil} = 400, Sc = \sqrt{48/18};$$

$$\text{SO}_2: \quad r_{water} = 0, r_{soil} = 1000, Sc = \sqrt{64/18};$$

$$\text{H}_2\text{O}_2: \quad r_{water} = 0, r_{soil} = 100, Sc = \sqrt{34/18}.$$

The method for calculating the dry deposition velocity of APM and FPM is based on the approach of Seinfeld and Pandis (1998). The deposition velocity is calculated using

$V_d = \frac{1}{r_{aH} + r_{bH} + r_{aH} r_{bH} V_s} + V_s$, where the resistance functions for heat transfer r_{aH} and r_{bH} and the particle settling velocity V_s are known, and the surface (water, soil, stomatal) resistance is assumed to be zero.

The quasi-laminar resistance r_{bH} accounts for Schmidt number (Sc) and Stokes number (St) dependence as follows:

$$r_{bH} = \frac{1}{u_* (Sc^{-2/3} + 10^{-3/St})}$$

with

$$Sc = \nu / D,$$

$$\nu = 1.58 \times 10^{-5} \text{ m}^2 \text{ s}^{-1},$$

$$D = \text{diffusivity of species} = \begin{cases} 6.10 \times 10^{-12} \text{ m}^2 \text{ s}^{-1} & \text{for APM,} \\ 2.74 \times 10^{-11} \text{ m}^2 \text{ s}^{-1} & \text{for FPM,} \end{cases}$$

and

$$St = \frac{V_s u_*^2}{g \nu},$$

$$V_s = \frac{g C_c \rho_p D_p^2}{18 \mu},$$

$$g = 9.81 \text{ m s}^{-2},$$

$$\rho_p = 1000 \text{ kg m}^{-3}, \mu = 1.8 \text{ kg m}^{-1} \text{ s}^{-1},$$

$$C_c = \begin{cases} 1.05 & \text{for APM,} \\ 1.16 & \text{for FPM,} \end{cases}$$

$$D_p = \text{representative particle aerodynamic diameter} = \begin{cases} 4 \mu\text{m} & \text{for APM,} \\ 1 \mu\text{m} & \text{for FPM.} \end{cases}$$

Wet deposition is important only for highly soluble gases and particles. For the pollutants considered in this model, the only ones removed by wet processes are APM, FPM, SO_2 , and H_2O_2 .

For the gases SO_2 and H_2O_2 , the amount of each pollutant dissolved in the rain-water fraction of the liquid water is computed for pollutant A as $[A]_R = (L_R R T K_{H_A}) [A]$, where $L_R = q_R \rho / \rho_w$ is the liquid rain-water volume fraction, R is the gas constant (0.082) in $\text{atm M}^{-1} \text{ K}^{-1}$, T is temperature in K, K_{H_A} is the effective Henry's Law coefficient for A , and concentrations are in ppb. $[A]_R$ is then vertically advected at the speed of the falling rain (V_T), to give $[A]_{R(NEW)}$. The new value of A is then $[A]_{(NEW)} = [A] - [A]_R + [A]_{R(NEW)}$.

For APM and FPM, the same approach is used as for the gases, except that we assume $K_{H_A} = K_{H_{MAX}} = (L_T R T)^{-1}$ (i.e. that all particles are dissolved in the available water), with the total liquid water volume fraction $L_T = (q_c + q_R) \rho / \rho_w$.

3.1.4 Emission correction factors

A range of pollutant emissions types can be used by the model. They include point sources, line sources, area sources and gridded surface sources. TAPM expects the seven optional gridded surface emission files to be in the following forms

- Gridded Surface Emissions (GSE), independent of meteorology;
- Biogenic Surface Emissions (BSE), at $T_{vege} = 30^\circ\text{C}$, $PAR = 1000 \mu\text{mol m}^{-2} \text{s}^{-1}$ for VOC;
- Wood Heater Emissions (WHE), at $T_{screen24} = 10^\circ\text{C}$ for all pollutant species;
- Vehicle Petrol eXhaust emissions (VPX), at $T_{screen} = 25^\circ\text{C}$ for VOC, NOX and CO;
- Vehicle Diesel eXhaust emissions (VDX), independent of meteorology;
- Vehicle Lpg eXhaust emissions (VLX), at $T_{screen} = 25^\circ\text{C}$ for VOC, NOX and CO;
- Vehicle Petrol eVaporative emissions (VPV), at $T_{screen} = 25^\circ\text{C}$ for VOC;

where T_{vege} is the vegetation temperature ($^\circ\text{C}$), PAR is the photo-synthetically active radiation ($\mu\text{mol m}^{-2} \text{s}^{-1}$), $T_{screen24}$ is a running 24-hour screen-level temperature ($^\circ\text{C}$), and T_{screen} is the screen-level temperature ($^\circ\text{C}$). The model adjusts the emissions throughout a simulation, according to predicted temperature and PAR.

The biogenic temperature and radiation corrections are from Guenther *et al.* (1993). The wood heater and vehicle temperature corrections used in the model are based on curve-fits to data described by Ng *et al.* (2000), which for vehicle emissions are based on the US model MOBILE5.

The temperature and radiation corrections for BSE emissions are

$$\text{VOC: } C_T = \frac{\exp\left(\frac{95000(T - 303.15)}{303.15RT}\right)}{1 + \exp\left(\frac{230000(T - 314)}{303.15RT}\right)},$$

$$C_{PAR} = \frac{1.066(0.0027PAR)}{\sqrt{1 + (0.0027PAR)^2}},$$

with

$$T = T_{vege} + 273.15,$$

$$R = 8.314 \text{ J K}^{-1} \text{ mol}^{-1},$$

$$PAR = 4.18 \cdot (0.55 \cdot TSR) \text{ in } \mu\text{mol m}^{-2} \text{ s}^{-1},$$

$$TSR = \text{total solar radiation (W m}^{-2}\text{)}.$$

The temperature correction for WHE emissions for all pollutant species is

$$C_T = \max(0, 2 - 0.1T_{screen24}).$$

The temperature corrections for VPX and VLX emissions are

$$\text{VOC: } C_T = \begin{cases} 1 - 0.03(T_{screen} - 25), & \text{if } T_{screen} < 25^\circ\text{C} \\ 1 + 0.02(T_{screen} - 25), & \text{if } T_{screen} \geq 25^\circ\text{C} \end{cases};$$

$$\text{NOX: } C_T = \begin{cases} 1 - 0.0125(T_{screen} - 25), & \text{if } T_{screen} < 25^\circ\text{C} \\ 1 - 0.0025(T_{screen} - 25), & \text{if } T_{screen} \geq 25^\circ\text{C} \end{cases};$$

$$\text{CO: } C_T = \begin{cases} 1 - 0.02(T_{\text{screen}} - 25), & \text{if } T_{\text{screen}} < 25^\circ\text{C} \\ 1 + 0.04(T_{\text{screen}} - 25), & \text{if } T_{\text{screen}} \geq 25^\circ\text{C} \end{cases}.$$

The temperature corrections for VPV emissions are

$$\text{VOC: } C_T = \begin{cases} \max(0.01, 1 + 0.05(\min(T_{\text{screen}}, 41) - 27)), & \text{if } T_{\text{screen}} < 27^\circ\text{C} \\ \max(0.01, 1 + 0.20(\min(T_{\text{screen}}, 41) - 27)), & \text{if } T_{\text{screen}} \geq 27^\circ\text{C} \end{cases}.$$

3.2 Lagrangian particle module

The Lagrangian Particle Module (LPM) can be used on the inner-most nest for selected point sources to allow a more detailed account of near-source effects, including gradual plume rise and near-source dispersion. The LPM uses a PARTPUFF approach as described by Hurley (1994), whereby mass is represented as a puff in the horizontal direction, and as a particle in the vertical direction. This configuration has been used successfully in the Lagrangian Atmospheric Dispersion Model (LADM, Physick *et al.*, 1994). Chemistry is accounted for in a straightforward coupled manner with the EGM, without having to convert secondary pollutant concentration back to particle mass. This is done by tracking primary emissions for a particular source with the LPM and accounting for reactions using the EGM (see later). Deposition processes are neglected in the LPM. Once particles have travelled for a certain length of time (model input), the particle is no longer tracked and its mass is converted to concentration and put onto the EGM grid.

3.2.1 Pollutant equations

In the horizontal directions, particle position is updated through advection by the ambient wind, with diffusion accounted for through a puff width relation based on statistical diffusion theory

$$\frac{d\sigma_y^2}{dt} = 2(\sigma_u^2 + \sigma_{up}^2) T_{Lu} \left(1 - \exp\left(-\frac{t}{T_{Lu}}\right) \right),$$

where

$\sigma_u^2, \sigma_{up}^2$ are the ambient and plume rise horizontal velocity variances respectively,

$$\sigma_u^2 = E - \frac{1}{2} \overline{w'^2},$$

σ_{up}^2 is specified in Section 3.3,

$T_{Lu} = \frac{2\sigma_u^2}{C_0 \epsilon}$ is the ambient horizontal Lagrangian timescale,

and $C_0 = 3.0$.

In the vertical direction, particle position is updated using

$$\frac{d\sigma_{\text{particle}}}{dt} = \dot{\sigma} + \dot{\sigma}' + \dot{\sigma}'_p,$$

where

$\sigma_{particle}$ is the particle position in terrain following coordinates,

$\dot{\sigma}$ is the mean ambient vertical velocity,

$\dot{\sigma}'$ is the perturbation of vertical velocity due to ambient turbulence,

$\dot{\sigma}'_p$ is the perturbation of vertical velocity due to plume rise effects.

Perfect reflection of particle vertical position and velocity is used at the ground.

The perturbation of vertical velocity due to ambient turbulence is determined from the solution of a Langevin equation using a non-stationary turbulence extension of the approach of Franzese *et al.* (1999)

$$\dot{\sigma}' = w' \frac{\partial \sigma}{\partial z},$$

$$dw' = (a_0 + a_1 w' + a_2 w'^2) dt + b_0 \xi,$$

where ξ is a random number from a Gaussian distribution with mean zero and variance one, and

$$b_0 = \sqrt{C_0 \mathcal{E} dt},$$

$$a_2 = \frac{\frac{1}{3} \left(\frac{\partial \overline{w'^3}}{\partial t} + \frac{\partial \overline{w'^4}}{\partial z} \right) - \frac{\overline{w'^3}}{2\overline{w'^2}} \left(\frac{\partial \overline{w'^2}}{\partial t} + \frac{\partial \overline{w'^3}}{\partial z} - C_0 \mathcal{E} \right) - \overline{w'^2} \frac{\partial \overline{w'^2}}{\partial z}}{\overline{w'^4} + \frac{(\overline{w'^3})^2}{\overline{w'^2}} + (\overline{w'^2})^2},$$

$$a_1 = \frac{1}{2\overline{w'^2}} \left(\frac{\partial \overline{w'^2}}{\partial t} + \frac{\partial \overline{w'^3}}{\partial z} - C_0 \mathcal{E} - 2\overline{w'^3} a_2 \right),$$

$$a_0 = \frac{\partial \overline{w'^2}}{\partial z} - \overline{w'^2} a_2.$$

Vertical velocity variance $\overline{w'^2}$ can be diagnosed from the following modified prognostic equation of Gibson and Launder (1978) and Andren (1990), when all advection and diffusion terms are neglected and the boundary-layer assumption is made (see Mellor and Yamada, 1982),

$$\overline{w'^2} = \left(\frac{2}{3} E + \frac{E}{c_{s1} \mathcal{E}} \left((2 - c_{s2} - c_{w2} \frac{l}{kz}) P_s + (2 - c_{s3} - c_{w3} \frac{l}{kz}) P_b - \frac{2}{3} \mathcal{E} \right) \right) \left(1 + \frac{c_{w1}}{c_{s1}} \frac{l}{kz} \right)^{-1},$$

with constants from Rodi (1985)

$$c_{s1} = 2.20, c_{s2} = 1.63, c_{s3} = 0.73, c_{w1} = 1.00, c_{w2} = 0.24, c_{w3} = 0.0.$$

Higher-order moments of the vertical velocity distribution $\overline{w'^3}$ and $\overline{w'^4}$ are determined from the vertical velocity variance using

$$\overline{w'^3} = 0.8 \left(\max(0, \overline{w'^2} - \overline{w'^2}_1) \right)^{3/2},$$

$$\overline{w'^4} = 3.5 \left(\overline{w'^2} \right)^2,$$

in the convective boundary layer, and Gaussian values used elsewhere

$$\overline{w'^3} = 0.0, \\ \overline{w'^4} = 3.0 \overline{(w'^2)^2}.$$

The subscript 1 here refers to the value of this variable at the first model level (10 m). This parameterisation produces a skewness of zero at the bottom and top of the convective boundary layer, and a peak value of about 0.6 within this layer. These parameterisations agree with measurements in the convective boundary layer as discussed by Luhar *et al.* (1996).

The perturbation of vertical velocity due to plume rise effects is determined using a random walk approach

$$\dot{\sigma}'_p = (w_p + \xi \sigma_{wp}) \frac{\partial \sigma}{\partial z},$$

where ξ is a random number from a Gaussian distribution with mean zero and variance one, and plume rise variables w_p and σ_{wp} are defined in Section 3.3.

In order to calculate total pollutant concentration for use in chemistry calculations and time-averaging, particles are converted to concentration at grid points of the EGM using the equation for the concentration increment of a particle at a grid point

$$\Delta\chi = \frac{\Delta m}{2\pi_c \sigma_y^2 \Delta z} \exp\left(-\frac{r^2}{2\sigma_y^2}\right),$$

where

Δm is the particle mass,

σ_y is the standard deviation of horizontal puff width,

Δz is the vertical grid spacing,

r is the horizontal distance from the particle position to the grid point.

3.2.2 Chemistry

In tracer mode, optional chemical decay of a particular pollutant is represented by exponentially decaying particle mass. In chemistry mode, pollutant emissions are converted to particle mass on release from the source, and stored for the variables APM, FPM, SO₂, NO_x, R_{smog}, SP_x and NO₂. Chemistry is accounted for in these variables by the EGM, except for the loss terms in the equation for SO₂, which are handled through an exponential decay of mass with reaction rate $k_{SO_2} = k_8[RP] + k_9[H_2O_2] + k_{10}[O_3]$. This reaction is then not computed in the EGM for the LPM component of SO₂. This approach allows the dispersion of the primary emissions of the above variables to be handled with the LPM, and avoids any dependence of the LPM on the EGM, except for the first order reaction rate of SO₂.

The diagnostic solution for the total concentration is then

$$[APM] = [APM]_{LPM} + [APM]_{EGM},$$

$$[FPM] = [FPM]_{LPM} + [FPM]_{EGM},$$

$$[SO_2] = [SO_2]_{LPM} + [SO_2]_{EGM},$$

$$[NO_X] = [NO_X]_{LPM} + [NO_X]_{EGM},$$

$$[R_{smog}] = [R_{smog}]_{LPM} + [R_{smog}]_{EGM},$$

$$[SP_X] = [SP_X]_{LPM} + [SP_X]_{EGM},$$

$$[NO_2] = [NO_2]_{LPM} + [NO_2]_{EGM},$$

$$[RP] = [RP]_{EGM},$$

$$[H_2O_2] = [H_2O_2]_{EGM}.$$

3.3 Plume rise module

The equations for mean plume rise of a point source emission are based on the model of Glendening *et al.* (1984), as simplified by Hurley and Manins (1995)

$$\frac{dG}{dt} = 2R(\alpha w_p^2 + \beta u_a w_p)$$

$$\frac{dF}{dt} = -\frac{sM}{u_p} \left(\frac{M}{M_{eff}} u_a + w_p \right)$$

$$\frac{dM}{dt} = F,$$

$$\frac{dx_p}{dt} = u,$$

$$\frac{dy_p}{dt} = v,$$

$$\frac{dz_p}{dt} = w_p,$$

with

$$G = \frac{T_a}{T_p} u_p R^2,$$

$$F = g u_p R^2 \left(1 - \frac{T_a}{T_p} \right)$$

$$M = \frac{T_a}{T_p} u_p R^2 w_p,$$

$$w_p = \frac{M}{G},$$

$$R = \sqrt{\frac{(G+F/g)}{u_p}},$$

$$u_p = \sqrt{u_a^2 + w_p^2},$$

$$u_a = \sqrt{u^2 + v^2},$$

G, F, M = plume volume, buoyancy, and momentum flux respectively,

R = plume radius (top - hat cross - section),

u, v, w = cartesian x, y, z components of velocity respectively,

T = temperature,

s = ambient buoyancy frequency,

subscript a refers to ambient variables, subscript p refers to plume variables,

$\alpha = 0.1$, $\beta = 0.6$, are vertical plume and bent - over plume entrainment constants respectively,

$\frac{M}{M_{eff}} = \frac{1}{2.25}$, g = gravitational constant (9.8 m s^{-2}).

Initial conditions for these equations are

$$G_o = \frac{T_a}{T_s} w_s R_s^2, F_o = N_E g w_s R_s^2 \left(1 - \frac{T_a}{T_s}\right) M_o = \frac{T_a}{T_s} w_s^2 R_s^2, R_o = \sqrt{\frac{w_s}{\sqrt{u_a^2 + w_s^2}}},$$

where N_E is the user-specified buoyancy enhancement factor (e.g., see Manins *et al.*, 1992, for parameterisations of N_E to handle overlapping plumes from multiple stacks), and subscript s representing stack exit conditions. Stack height is adjusted for stack-tip downwash following Briggs (1973): $h_{sd} = h_s - 4R_s \max\left(0, 1.5 - \frac{w_s}{u_a}\right)$.

Plume rise is terminated when the plume dissipation rate decreases to ambient levels.

Tests of these equations against both the full Glendening and the Briggs (1975) form of the plume rise equations by Hurley and Manins (1995), showed that the above form was just as good as the full Glendening form for all conditions. Our form also collapses to the Briggs form for a bent-over Boussinesq plume, and to the Briggs vertical plume model equations for zero ambient wind. It was also found that for very hot plumes in a bent-over plume situation, the Briggs form was very close to our form, even though the Boussinesq approximation was not strictly valid. This finding is probably due to the rapid decrease of plume temperature excess with travel time.

In the EGM, plume rise for a point source is accounted for by releasing pollutants at the effective source height as calculated by the above equations, with a plume depth that assumes a 2:1 horizontal to vertical plume shape, and that the plume radius for concentration is two-thirds that of the visual radius R above. Pollutant emissions are then distributed uniformly to grid points within the plume depth at the nearest horizontal grid point (assuming plume width is always sub-grid scale).

In the LPM, a gradual plume rise approach is used with a random component that depends on the standard deviation of the vertical velocity due to plume rise effects, and an enhanced horizontal spread. The standard deviations of velocity assume a slightly simplified form of the above equation for G , a 2:1 horizontal to vertical plume shape, a plume radius for concentration of two-thirds the visual radius R , and a standard deviation half that of the radius. This results in the equations

$$\sigma_{wp} = \frac{\alpha w_p^2 + \beta u_a w_p}{3\sqrt{2}u_p}, \text{ and } \sigma_{up} = 2\sigma_{wp}.$$

3.4 Building wake module

The effect of building wakes on plume rise and dispersion is based on the Plume Rise Model Enhancements (PRIME) approach of Schulman *et al.* (2000). The PRIME model uses an along-wind coordinate system, and so first each building is transformed to be in this system. Effective building dimensions and cavity and wake dimensions are then calculated for each building and are then used to determine the combined wake meteorology and turbulence. Plume rise is affected by the modified meteorology and turbulence for point sources in both EGM and LPM modes, while dispersion is influenced only for plumes in LPM mode. LPM

calculations are done for both the cavity and wake regions, rather than specifying a uniform concentration in the cavity as is done in PRIME.

3.4.1 Transformation to along-wind coordinate system

Using the local horizontal wind components (u, v) in a Cartesian coordinate system, a point (x, y) can be rotated to be in an along-wind coordinate system (x', y') by using the transformation

$$x' = (xu - yv)/U \text{ and } y' = (yu - xv)/U, \text{ with } U = \sqrt{u^2 + v^2}.$$

The horizontal coordinates of the building corners are converted to be in the along-wind coordinate system, using the above transformation. Then, after calculating the minimum and maximum corner point coordinate components, the effective building dimensions are calculated as length $L = x'_{\max} - x'_{\min}$ and width $W = y'_{\max} - y'_{\min}$. We then define the origin for this building at the centre of the upwind face of the building $(x'_0, y'_0) = (x'_{\min}, \frac{1}{2}(y'_{\min} + y'_{\max}))$.

3.4.2 Building wake dimensions

Given an effective building length (L), width (W) and height (H) in an along-wind coordinate system (x, y, z) (m) with origin at the centre of the upwind face of the building, a diffusion length scale (R) is

$$R = B_S^{2/3} B_L^{1/3}, \text{ with } B_S = \min(H, W) \text{ and } B_L = \min(8B_S, \max(H, W)).$$

The maximum height of the cavity (recirculation zone) is then

$$H_R = \begin{cases} H, & \text{if } L > 0.9R \text{ (reattachment)} \\ H + 0.22R, & \text{otherwise} \end{cases},$$

and the length of the cavity from the lee-face of the building is

$$L_R = \frac{1.8W}{\left(\max\left(0.3, \min\left(\frac{L}{H}, 3 \right) \right) \right)^{0.3} \left(1 + 0.24 \frac{W}{H} \right)}.$$

The cavity height is

$$H_c(x) = \begin{cases} \begin{cases} H, & \text{if } 0 < x \leq L \\ H \left(1 - \left(\frac{x-L}{L_R} \right)^2 \right), & \text{if } L < x < L + L_R \end{cases}, & \text{if } L > 0.9R \\ \begin{cases} H_R + \frac{4(x-0.5R)^2(H-H_R)}{R^2}, & \text{if } 0 < x \leq 0.5R \\ H_R \left(1 - \frac{(x-0.5R)^2}{(L+L_R-0.5R)^2} \right)^{0.5}, & \text{if } 0.5R < x < L + L_R \end{cases}, & \text{otherwise} \end{cases}$$

and the cavity width is

$$W_c(x) = \begin{cases} \frac{W}{2} + \frac{R}{3} - \frac{(x-R)^2}{3R}, & \text{if } 0 < x \leq R \\ \left(\frac{W}{2} + \frac{R}{3}\right) \sqrt{1 - \left(\frac{x-R}{L+L_R}\right)^2}, & \text{if } R < x < L + L_R \end{cases}.$$

The wake height is

$$H_w(x) = 1.2R \left(\frac{x}{R} + \left(\frac{H}{1.2R} \right)^3 \right)^{1/3}$$

and the wake width is

$$W_w(x) = \frac{W}{2} + \frac{R}{3} \left(\frac{x}{R} \right)^{1/3}.$$

3.4.3 Building wake meteorology and turbulence

The meteorology and turbulence characteristics described below are used in the calculation of concentration in the following Sections.

Streamline slope over a building is calculated in along-wind coordinates as

$$\left(\frac{dz}{dx} \right)_{wake}(x) = \begin{cases} 0, & \text{if } x < -R \\ \frac{F_z 2(H_R - H)(x + R)}{R^2}, & \text{if } -R \leq x < 0 \\ \frac{F_z 4(H_R - H)(R - 2x)}{R^2}, & \text{if } 0 \leq x < 0.5R \\ \frac{F_z (H_R - H)(R - 2x)}{(L + L_R - 0.5R)^2} \left(\frac{z}{H} \right)^{0.3}, & \text{if } 0.5R \leq x < L + L_R \\ \frac{F_z (H_R - H)(R - 2(L + L_R))}{(L + L_R - 0.5R)^2} \left(\frac{z}{H} \right)^{0.3} \left(\frac{L + L_R}{x} \right), & \text{if } x \geq L + L_R \end{cases}$$

with $F_z = 1$ if $z \leq H$, and if $z > H$ then

$$F_z = \begin{cases} 1, & \text{if } x < -R \\ \left(\frac{H}{z} \right)^3, & \text{if } -R \leq x < 0.5R \\ \left(\frac{H}{z} \right), & \text{if } x \geq R \end{cases}.$$

The horizontal wind speed factor F_U and the turbulence intensities i_x and i_z are calculated as follows.

If $x \leq L + L_R$ and $z \leq H_R$

$$F_U = F_C,$$

$$F_C = \max\left(0.1, 1 - \frac{\frac{\Delta U}{U} H_W}{0.5(H_C + H_W)}\right),$$

$$i_z = i_{zc} / \left(1 - \frac{\Delta U}{U}\right),$$

$$i_x = 0.5 \max\left(0.3, \min\left(\frac{W}{H}, 3\right)\right),$$

otherwise if $z \leq H_W$

$$F_U = F_C + (1 - F_C) \frac{(z - H_C)}{(H_W - H_C)},$$

$$F_C = \max\left(0.1, 1 - \frac{F_x \frac{\Delta U}{U} H_W}{0.5(H_C + H_W)}\right),$$

$$i_z = 1.7 i_{zN} \left(\frac{F_x}{1 - F_x \frac{\Delta U}{U}} \right),$$

$$i_x = i_z,$$

$$F_x = \begin{cases} \left(\frac{x}{L}\right)^{2/3}, & \text{if } 0 < x < L \\ \left(\frac{R}{x - L + R}\right)^{2/3}, & \text{if } x \geq L \end{cases},$$

with $\frac{\Delta U}{U} = 0.7$, $i_{zc} = 1.0$ and $i_{zN} = 0.06$.

Note that we have parameterised cavity turbulence, and do not assume a uniform cavity concentration as is done in PRIME. Note also that wake calculations are done only if $x < 15R$ and $|y| < 0.5W_W$.

3.4.4 Treatment of multiple building blocks

If we define a building block as having a constant height H , then we can use the above procedure to define wake characteristics for each building block. The effects of overlapping wakes from multiple building blocks, whether from the same multi-level or multi-tiered physical building, or from multiple physical buildings, can be treated by combining the meteorology and turbulence. For a particular point in space, the combined (over all building blocks)

- streamline slope can be calculated by first calculating the maximum slope and the minimum slope, and then if the absolute value of the maximum is greater than the absolute value of the minimum, then use the maximum value, otherwise use the minimum value;
- horizontal wind speed factor is the minimum value;
- turbulence intensity is the maximum value.

The combined effects can then be used for the calculation of plume rise and dispersion – the above approach attempts to be conservative for expected ground-level pollution concentration.

3.4.5 Wake effects on plume rise

For the calculation of plume rise (Section 3.3), the horizontal wind and the differential equations for G and z_p are adjusted as follows

$$u = u_{old} F_U, v = v_{old} F_U \text{ and then } U = \sqrt{u^2 + v^2},$$

$$\frac{dG}{dt} = \max\left(\frac{dG}{dt}\bigg|_{old}, \sqrt{\frac{\pi_c}{2}} U^2 i_z\right),$$

$$\frac{dz_p}{dt} = \frac{dz_p}{dt}\bigg|_{old} + U \left(\frac{dz}{dx}\right)_{wake}.$$

3.4.6 Wake effects on LPM dispersion

For LPM dispersion, the mean wind is modified

$$u = u_{old} F_U, v = v_{old} F_U \text{ and then } U = \sqrt{u^2 + v^2}, \text{ and } w = w_{old} + U \left(\frac{dz}{dx}\right)_{wake},$$

while the horizontal plume spread incorporates an extra term using $\sigma_u = U i_x$ and the LPM random-walk equation also includes a contribution from $\sigma_w = U i_z$.

4 Numerical methods

The flow chart in Figure 1 illustrates the order of calculations in the model. The model uses a large timestep of 300 s on which radiation and surface processes are calculated. Meteorological and turbulence equations are solved with a timestep of $\Delta t_M = \frac{1}{U_M} \min(\Delta x_M, \Delta y_M)$, where U_M is a characteristic wind speed ($U_M = 30 \text{ m s}^{-1}$ is the model default), and Δx_M and Δy_M are the horizontal grid spacings in metres on the meteorological grid. Pollution concentration equations for the EGM are solved with a timestep of $\Delta t_P = \frac{1}{U_P} \min(\Delta x_P, \Delta y_P)$, where $U_P = 0.5 U_M$, and Δx_P and Δy_P are the horizontal grid spacings in metres on the pollution grid. The pollution grid can be a subset of the meteorological grid at finer grid spacing. The maximum synoptic wind speed used by the model is set to be U_M , in order to avoid Courant numbers being too much greater than 1 for the meteorology. This restriction was found to be important for the reduction of numerical error, particularly near the model top and in non-hydrostatic mode.

Model equations are solved using finite difference methods with no grid stagger, a constant grid spacing in the horizontal directions, and a variable grid spacing in the vertical direction. Second-order centred spatial differencing is used, for example

$$\left.\frac{\partial \phi}{\partial x}\right|_i = \frac{1}{2\Delta x} (\phi_{i+1} - \phi_{i-1}),$$

$$\left.\frac{\partial \phi}{\partial y}\right|_j = \frac{1}{2\Delta y} (\phi_{j+1} - \phi_{j-1}),$$

$$\begin{aligned}
 \frac{\partial \phi}{\partial \sigma}_k &= \frac{1}{(\sigma_{k+1} - \sigma_{k-1})} \left(\left(\frac{\sigma_k - \sigma_{k-1}}{\sigma_{k+1} - \sigma_k} \right) (\phi_{k+1} - \phi_k) + \left(\frac{\sigma_{k+1} - \sigma_k}{\sigma_k - \sigma_{k-1}} \right) (\phi_k - \phi_{k-1}) \right), \\
 \frac{\partial}{\partial x} \left(K \frac{\partial \phi}{\partial x} \right)_i &= \frac{1}{2(\Delta x)^2} ((K_{i+1} + K_i)(\phi_{i+1} - \phi_i) - (K_i + K_{i-1})(\phi_i - \phi_{i-1})), \\
 \frac{\partial}{\partial y} \left(K \frac{\partial \phi}{\partial y} \right)_j &= \frac{1}{2(\Delta y)^2} ((K_{j+1} + K_j)(\phi_{j+1} - \phi_j) - (K_j + K_{j-1})(\phi_j - \phi_{j-1})), \\
 \frac{\partial}{\partial \sigma} \left(K \frac{\partial \phi}{\partial \sigma} \right)_k &= \frac{1}{(\sigma_{k+1} - \sigma_{k-1})} \left(\left(\frac{K_{k+1} + K_k}{\sigma_{k+1} - \sigma_k} \right) (\phi_{k+1} - \phi_k) - \left(\frac{K_k + K_{k-1}}{\sigma_k - \sigma_{k-1}} \right) (\phi_k - \phi_{k-1}) \right).
 \end{aligned}$$

4.1 Horizontal advection

Horizontal advection for all prognostic variables is calculated with timesteps Δt_M or Δt_P using the semi-Lagrangian technique of McGregor (1993) with the quasi-monotone conversion of Bermejo and Staniforth (1992). To $O((\Delta t)^2)$, the departure point (i_*, j_*) in grid units can be determined for horizontal grid point (i, j) from

$$i_* = i - u_{i,j}^{n+1/2} \frac{\Delta t}{\Delta x} + \frac{(\Delta t)^2}{2\Delta x} \left(u \frac{\partial u}{\partial x} + v \frac{\partial u}{\partial y} \right)_{i,j}^{n+1/2},$$

$$j_* = j - v_{i,j}^{n+1/2} \frac{\Delta t}{\Delta y} + \frac{(\Delta t)^2}{2\Delta y} \left(u \frac{\partial u}{\partial x} + v \frac{\partial u}{\partial y} \right)_{i,j}^{n+1/2},$$

with $u_{i,j}^{n+1/2} = 1.5u_{i,j}^n - 0.5u_{i,j}^{n-1}$ or $u_{i,j}^{n+f} = fu_{i,j}^{n+1} + (1-f)u_{i,j}^n$ and similarly for v , for the meteorological and concentration variables respectively (f accounts for fractional timesteps). Each prognostic variable can then be determined from $\phi_{i,j}^{n+1} = \phi_{i_*, j_*}^n$ using Lagrange cubic polynomial interpolation separately in each coordinate direction.

Defining $i = \text{int}(i_*)$ and $x_* = i_* - i$, then

$$\begin{aligned}
 \phi_{i,j}^n &= -\frac{1}{6} x_* (x_* - 1)(x_* - 2)\phi_{i-1,j}^n + \frac{1}{2} (x_*^2 - 1)(x_* - 2)\phi_{i,j}^n \\
 &\quad - \frac{1}{2} x_* (x_* + 1)(x_* - 2)\phi_{i+1,j}^n + \frac{1}{6} x_* (x_*^2 - 1)\phi_{i+2,j}^n,
 \end{aligned}$$

subject to $\min(\phi_{i,j}^n, \phi_{i+1,j}^n) \leq \phi_{i,j}^n \leq \max(\phi_{i,j}^n, \phi_{i+1,j}^n)$.

Similarly, if $j = \text{int}(j_*)$ and $y_* = j_* - j$, then

$$\begin{aligned}
 \phi_{i,j}^n &= -\frac{1}{6} y_* (y_* - 1)(y_* - 2)\phi_{i,j-1}^n + \frac{1}{2} (y_*^2 - 1)(y_* - 2)\phi_{i,j}^n \\
 &\quad - \frac{1}{2} y_* (y_* + 1)(y_* - 2)\phi_{i,j+1}^n + \frac{1}{6} y_* (y_*^2 - 1)\phi_{i,j+2}^n,
 \end{aligned}$$

subject to $\min(\phi_{i,j}^n, \phi_{i,j+1}^n) \leq \phi_{i,j}^n \leq \max(\phi_{i,j}^n, \phi_{i,j+1}^n)$.

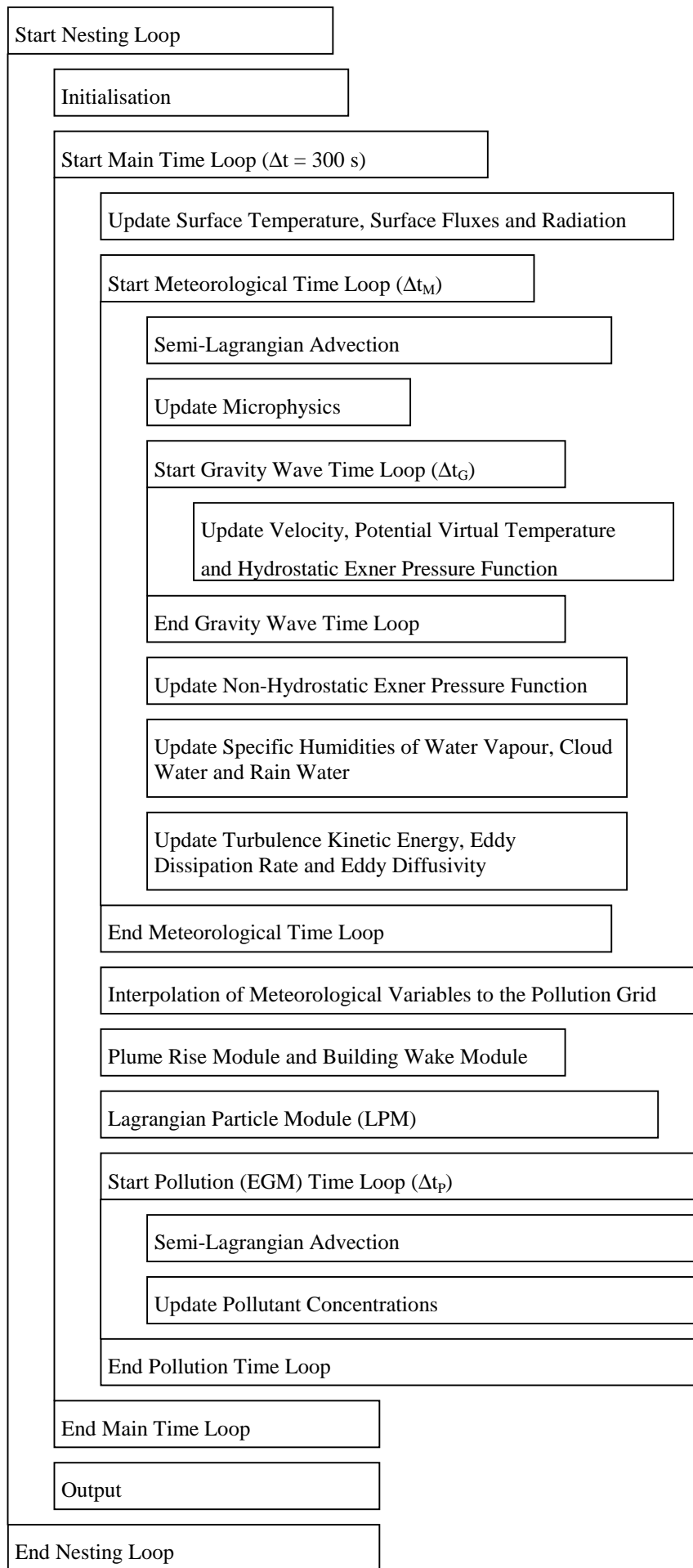


Figure 1. Flow chart of TAPM.

4.2 Vertical advection

Vertical advection for all prognostic variables except θ_v , is calculated with timesteps Δt_M or Δt_P using the semi-Lagrangian technique of McGregor (1993) with the quasi-monotone conversion of Bermejo and Staniforth (1992). To $O((\Delta t)^2)$, the departure point can be determined from

$$\sigma_* = \sigma_k - \dot{\sigma}_k^{n+1/2} \Delta t + \frac{1}{2} (\Delta t)^2 \left(\dot{\sigma} \frac{\partial \dot{\sigma}}{\partial \sigma} \right)_k^{n+1/2},$$

with $\dot{\sigma}_k^{n+1/2} = 1.5\dot{\sigma}_k^n - 0.5\dot{\sigma}_k^{n-1}$ or $\dot{\sigma}_k^{n+f} = f\dot{\sigma}_k^{n+1} + (1-f)\dot{\sigma}_k^n$, for the meteorological and concentration variables respectively (f accounts for fractional timesteps). Each prognostic variable can then be determined from $\phi_k^{n+1} = \phi_{k_*}^n$ (where k denotes the nearest model level to σ_* that satisfies $\sigma_k \leq \sigma_*$), using Lagrange cubic polynomial interpolation (with quasi-monotone conversion)

$$\begin{aligned} \phi_{k_*}^n = & \left(\frac{\sigma_* - \sigma_k}{\sigma_{k-1} - \sigma_k} \right) \left(\frac{\sigma_* - \sigma_{k+1}}{\sigma_{k-1} - \sigma_{k+1}} \right) \left(\frac{\sigma_* - \sigma_{k+2}}{\sigma_{k-1} - \sigma_{k+2}} \right) \phi_{k-1}^n \\ & + \left(\frac{\sigma_* - \sigma_{k-1}}{\sigma_k - \sigma_{k-1}} \right) \left(\frac{\sigma_* - \sigma_{k+1}}{\sigma_k - \sigma_{k+1}} \right) \left(\frac{\sigma_* - \sigma_{k+2}}{\sigma_k - \sigma_{k+2}} \right) \phi_k^n \\ & + \left(\frac{\sigma_* - \sigma_{k-1}}{\sigma_{k+1} - \sigma_{k-1}} \right) \left(\frac{\sigma_* - \sigma_k}{\sigma_{k+1} - \sigma_k} \right) \left(\frac{\sigma_* - \sigma_{k+2}}{\sigma_{k+1} - \sigma_{k+2}} \right) \phi_{k+1}^n \\ & + \left(\frac{\sigma_* - \sigma_{k-1}}{\sigma_{k+2} - \sigma_{k-1}} \right) \left(\frac{\sigma_* - \sigma_k}{\sigma_{k+2} - \sigma_k} \right) \left(\frac{\sigma_* - \sigma_{k+1}}{\sigma_{k+2} - \sigma_{k+1}} \right) \phi_{k+2}^n, \end{aligned}$$

subject to $\min(\phi_k^n, \phi_{k+1}^n) \leq \phi_{k_*}^n \leq \max(\phi_k^n, \phi_{k+1}^n)$.

4.3 Gravity waves

The equations for the meteorological variables $u, v, \dot{\sigma}, \theta_v$, and π_H are solved by using a time-split approach where gravity wave terms are separated from the others and solved on a small timestep $\Delta t_G = \frac{1}{U_G} \min(\Delta x_M, \Delta y_M)$, where $U_G = 120 \text{ m s}^{-1}$ (note that $U_G = 140 \text{ m s}^{-1}$ for grid spacing below 1000 m)

$$\begin{aligned} \frac{\partial u}{\partial t} &= -\theta_v \frac{\partial \pi_H}{\partial x} + R_u, \\ \frac{\partial v}{\partial t} &= -\theta_v \frac{\partial \pi_H}{\partial y} + R_v, \\ \frac{\partial \dot{\sigma}}{\partial \sigma} &= -\left(\frac{\partial u}{\partial x} + \frac{\partial v}{\partial y} \right) + u \frac{\partial^2 \sigma}{\partial \sigma \partial x} + v \frac{\partial^2 \sigma}{\partial \sigma \partial y}, \end{aligned}$$

$$\frac{\partial \theta_v}{\partial t} = -\dot{\sigma} \frac{\partial \theta_v}{\partial \sigma} + R_{\theta_v},$$

$$\frac{\partial \pi_H}{\partial \sigma} = -\frac{g}{\theta_v} \left(\frac{\partial \sigma}{\partial z} \right)^{-1},$$

with R_u , R_v , and R_{θ_v} (updated on the timestep Δt_M)

$$R_u = g \frac{\partial \sigma}{\partial x} \left(\frac{\partial \sigma}{\partial z} \right)^{-1} + f(v - v_s) - N_s(u - u_s) - \theta_v \left(\frac{\partial \pi_N}{\partial x} + \frac{\partial \pi_N}{\partial \sigma} \frac{\partial \sigma}{\partial x} \right),$$

$$R_v = g \frac{\partial \sigma}{\partial y} \left(\frac{\partial \sigma}{\partial z} \right)^{-1} - f(u - u_s) - N_s(v - v_s) - \theta_v \left(\frac{\partial \pi_N}{\partial y} + \frac{\partial \pi_N}{\partial \sigma} \frac{\partial \sigma}{\partial y} \right),$$

$$R_{\theta_v} = S_{\theta_v} - \gamma_{cg} \frac{\partial K}{\partial \sigma} \frac{\partial \sigma}{\partial z} - N_s(\theta_v - \theta_{vs}),$$

and also include the nesting terms.

These prognostic equations are solved using the second-order Adams-Bashforth scheme

$$u^{n+1} = u^n + \frac{\Delta t}{2} \left(3 \frac{\partial u}{\partial t} \Big|_n - \frac{\partial u}{\partial t} \Big|^{n-1} \right),$$

while diagnostic vertical integration using the trapezoidal rule is performed from the ground to the model top to obtain $\dot{\sigma}$, and from the model top to the ground to obtain π_H .

On the timestep Δt_G , an implicit tri-diagonal horizontal filter described by Pielke (1984) is used instead of horizontal diffusion. The filter, represented by $F(\phi)$ in equations 1, 2 and 4 of Section 2.1, is applied separately in each horizontal direction with a filter coefficient of $\delta = 0.10$ (increased values are used near the top of the model). The equations solved are

$$(1 - \delta) \phi_{i-1,j}^{n+1} + 2(1 + \delta) \phi_{ij}^{n+1} + (1 - \delta) \phi_{i+1,j}^{n+1} = \phi_{i-1,j}^n + 2\phi_{ij}^n + \phi_{i+1,j}^n,$$

$$(1 - \delta) \phi_{ij-1}^{n+1} + 2(1 + \delta) \phi_{ij}^{n+1} + (1 - \delta) \phi_{ij+1}^{n+1} = \phi_{ij-1}^n + 2\phi_{ij}^n + \phi_{ij+1}^n.$$

On the timestep Δt_M , vertical diffusion is solved using a first-order implicit approach with special treatment of fluxes at the surface boundary (see next section).

4.4 Scalar prognostic equations

All other prognostic equations including those for specific humidity, turbulence, and pollutant concentrations, are of the general form for variable χ

$$\frac{\partial \chi}{\partial t} = \left(\frac{\partial \sigma}{\partial z} \right)^2 \frac{\partial}{\partial \sigma} \left(K \frac{\partial \chi}{\partial \sigma} \right) + RHS_1 - \chi RHS_2.$$

This equation is solved using first-order time differencing with a semi-implicit approach to give the equation

$$(1 + \Delta t RHS_2) \chi^{n+1} - \Delta t \left(\frac{\partial \sigma}{\partial z} \right)^2 \frac{\partial}{\partial \sigma} \left(K \frac{\partial \chi^{n+1}}{\partial \sigma} \right) = \chi^n + \Delta t RHS_1,$$

which can be solved as follows (with special treatment of fluxes at the surface) using a tri-diagonal solution method if second-order spatial differencing is used

$$A\chi_{k-1}^{n+1} + B\chi_k^{n+1} + C\chi_{k+1}^{n+1} = D;$$

if $k > 1$:

$$A = -\left(\frac{\partial\sigma}{\partial z}\right)^2 \frac{\Delta t}{(\sigma_{k+1} - \sigma_{k-1})} \left(\frac{K_k + K_{k-1}}{\sigma_k - \sigma_{k-1}} \right),$$

$$C = -\left(\frac{\partial\sigma}{\partial z}\right)^2 \frac{\Delta t}{(\sigma_{k+1} - \sigma_{k-1})} \left(\frac{K_{k+1} + K_k}{\sigma_{k+1} - \sigma_k} \right),$$

$$B = 1 + \Delta t RHS_2 - A - C,$$

$$D = \chi_k^n + \Delta t RHS_1;$$

if $k = 1$:

$$A = 0,$$

$$C = -\frac{1}{2} \left(\frac{\partial\sigma}{\partial z} \right)^2 \frac{\Delta t}{(\sigma_{3/2} - \sigma_0)} \left(\frac{K_2 + K_1}{\sigma_2 - \sigma_1} \right),$$

$$B = 1 + \Delta t RHS_2 - C,$$

$$D = \chi_1^n + \Delta t RHS_1 - \Delta t \left(\frac{\partial\sigma}{\partial z} \right) \frac{\text{flux}(\chi)}{(\sigma_{3/2} - \sigma_0)},$$

with $\text{flux}(\chi) = u_* \chi_*$ or $\text{flux}(\chi) = V_d \chi_1$.

The value of RHS_2 is non-zero only for the ε equation, the $\overline{\theta'_v \chi'}$ equations, and the SO₂, NO₂, RP and H₂O₂ pollutant concentration equations, where the loss terms are treated implicitly. The RHS_1 term includes all other terms in the particular prognostic equations, including explicit horizontal diffusion. The non-zero RHS_2 terms are

$$\varepsilon : RHS_2 = c_{\varepsilon 2} \frac{\varepsilon}{E},$$

$$\overline{\theta'_v \chi'} : RHS_2 = \frac{2}{c_\chi} \frac{\varepsilon}{E},$$

$$[SO_2] : RHS_2 = k_8[RP] + k_9[H_2O_2] + k_{10}[O_3],$$

$$[NO_2] : RHS_2 = k_3 + k_4([NO_x] + [SP_x] - [NO_2]),$$

$$[RP] : RHS_2 = k_2[NO] + k_5[RP] + (k_6 + k_7)[NO_2] + k_8[SO_2],$$

$$[H_2O_2] : RHS_2 = k_9[SO_2].$$

When the stability criterion for explicit horizontal diffusion of pollution variables is breached, the solution dynamically switches to an unconditionally stable implicit mode analogous to that used for vertical diffusion.

4.5 Other methods

- On the timestep Δt_M , the elliptic non-hydrostatic pressure perturbation equation is solved using an iterative approach. The solution is performed only for a sub-grid region that

excludes the 5 edge grid points at the top and lateral boundaries, as these edge regions usually contain noisy solutions which can produce spurious vertical velocities to which the non-hydrostatic solution is highly sensitive.

- For numerical representation of the vertical fluxes, it is necessary to use a finite difference approximation consistent with that used for the vertical diffusion

$$\overline{w' \chi'}_k = -\frac{1}{2}(K_{k+1} + K_k) \left(\frac{\sigma_k - \sigma_{k-1}}{\sigma_{k+1} - \sigma_{k-1}} \right) \left(\frac{\chi_{k+1} - \chi_k}{\sigma_{k+1} - \sigma_k} \right) \left(\frac{\partial \sigma}{\partial z} \right) \\ - \frac{1}{2}(K_k + K_{k-1}) \left(\frac{\sigma_{k+1} - \sigma_k}{\sigma_{k+1} - \sigma_{k-1}} \right) \left(\frac{\chi_k - \chi_{k-1}}{\sigma_k - \sigma_{k-1}} \right) \left(\frac{\partial \sigma}{\partial z} \right).$$

- At times of rapid variations in the surface temperature and specific humidity (such as just after sunrise), the surface heat balance approach used for vegetation can produce oscillations. Therefore, the vegetation temperature and moisture are time averaged using the current and previous values to prevent the oscillations.
- Linear interpolation is used to convert the synoptic-scale variables from the gridded analyses to the model.
- The plume rise equations are solved using the fourth-order Runge-Kutta method with a timestep of 1 second.
- The LPM uses explicit, forward in time finite differences and centred in space finite differences, with a large timestep of $\Delta t_{LPM} = 2\Delta t_P$ and a small timestep of 5 seconds for the solution in the vertical direction.
- The turbulence production/dissipation balance and wet processes are handled separately on a small timestep of 100 s.
- For multi-dimensional simulations, it was found necessary to bound the value of the length scale in order to keep the numerical solution stable for the ε prognostic equation. Also, the counter-gradient tracer flux and cross-correlation term are restricted to be zero in thermally stable regions, and are bounded elsewhere.

5 Acknowledgments

Some of the methodologies and parameterisations used in TAPM have also been used in the Lagrangian Atmospheric Dispersion Model (LADM) of Physick *et al.* (1994), and experience gained by working with other team members on developing and applying LADM has proved to be invaluable in the development of TAPM.

The encouragement, advice and suggestions for improvements from Bill Physick, Peter Manins, Mark Hibberd, Ashok Luhar, Julie Noonan and Martin Cope on TAPM is much appreciated. Helpful comments from many other people in CSIRO Atmospheric Research, CSIRO Energy Technology and CSIRO Land and Water on various aspects of this work, including the implementation of some of the model parameterisations, are gratefully acknowledged. The suggestions for improving/extending TAPM by model users has also been invaluable in the development of TAPM Version 2.0.

6 References

Andren A. (1990). 'Evaluation of a turbulence closure scheme suitable for air pollution applications', *J. Appl. Meteorol.*, **29**, 224-239.

Azzi M., Johnson G.M., and Cope M. (1992). 'An introduction to the generic reaction set photochemical smog mechanism', *Proceedings of the 11th International Clean Air and Environment Conference*, Brisbane, 1992, Clean Air Society of Australia & New Zealand.

Baines P.G., and Murray D. (1991). 'Modelling of the airflow over Cape Grim', *Baseline 91*, 20-24.

Bermejo R., and Staniforth A. (1992). 'The conversion of semi-Lagrangian schemes to quasi-monotone schemes', *Mon. Wea. Rev.* **120**, 2622-2632.

Briggs G.A. (1973). 'Diffusion estimation for small emissions', ATDL No 79, Atmospheric Turbulent Diffusion Laboratory, NOAA Environmental Resources Laboratory, Oak Ridge, Tennessee.

Briggs G.A. (1975). 'Plume Rise Predictions. In *Lectures on Air Pollution and Environmental Impact Analysis*', Ed. D.A. Haugen, AMS, Boston, MA, pp. 59-111.

Briggs G.A. (1985). 'Analytic parameterisations of diffusion : the convective boundary layer', *J. Clim. & Appl. Meteorol.*, **24**, 1167-1186.

Davies H. (1976). 'A lateral boundary formulation for multi-level prediction models', *Q. J. R. Meteorol. Soc.* **102**, 405-418.

Deardorff J.W. (1966). 'The counter-gradient heat flux in the lower atmosphere and in the laboratory', *J. Atmos. Sci.*, **23**, 503-506.

Derbyshire S.H. (1990). 'Nieuwstadt's stable boundary layer revisited', *Q. J. R. Meteorol. Soc.* **116**, 127-158.

Dilley A.C., and O'Brien D.M. (1999). 'Estimating downward clear-sky long-wave irradiance at the surface from screen temperature and precipitable water', *Submitted to Q. J. R. Meteorol. Soc.*

Duynkerke P.G. (1988). 'Application of the E - ε turbulence closure model to the neutral and stable atmospheric boundary layer', *J. Atmos. Sci.*, **45**, 865-880.

Duynkerke P.G., and Driedonks A.G.M. (1987). 'A model for the turbulent structure of the stratocumulus-topped atmospheric boundary layer', *J. Atmos. Sci.*, **44**, 43-64.

Dyer A.J., and Hicks B.B. (1970). 'Flux-gradient relationships in the constant flux layer', *Quart. J. Roy. Meteorol. Soc.*, **96**, 715-721.

Enger L. (1986). 'A higher order closure model applied to dispersion in a convective pbl', *Atmos. Environ.*, **20**, 879-894.

Franzese P., Luhar A.K., and Borgas M.S. (1999). 'An efficient Lagrangian stochastic model of vertical dispersion in the convective boundary layer.' *Atmos. Environ.*, **33**, 2337-2345.

Garratt J.R. (1992). 'The atmospheric boundary layer', Cambridge atmospheric and space science series, Cambridge University Press, Cambridge, 316 pp.

Gibson M.M., and Launder B.E. (1978). 'Ground effects on pressure fluctuations in the atmospheric boundary layer', *J. Fluid Mech.*, **86**, 491-511.

Glendening J.W., Businger J.A., and Farber R.J. (1984). 'Improving Plume Rise Prediction Accuracy for Stable Atmospheres with Complex Vertical Structure', *J. Air Pollut. Control Ass.*, **34**, pp. 1128-1133.

Guenther A., Zimmerman P., Harley P., Monson R. and Fall R. (1993). 'Isoprene and monoterpene emission rate variability: Model evaluations and sensitivity analyses.' *J. Geophys. Res.*, **98**, 12609-12617.

Harley R.A., Russell A.G., McRae G.J., Cass G.R. & Seinfeld J.H. (1993). 'Photochemical modelling of the southern California air quality study', *Environ. Sci. Technol.*, **27**, 378-388.

Hurley, P.J. (1994). 'PARTPUFF - A Lagrangian particle/puff approach for plume dispersion modelling applications', *J. Appl. Meteorol.*, **33**, 285-294.

Hurley P.J., and Manins P.C. (1995). 'Plume rise and enhanced dispersion in LADM'. CSIRO Atmospheric Research, ECRU Technical Note No. 4. 4 pp.

Hurley P., Physick W. and Luhar A. (2002). 'The Air Pollution Model (TAPM) Version 2. Part 2: Summary of some verification studies', CSIRO Atmospheric Research Technical Paper No. ???. ?? pp.

Johnson G.M. (1984). 'A simple model for predicting the ozone concentration of ambient air', *Proceedings of the 8th International Clean Air and Environment Conference*, New Zealand, 1984, Clean Air Society of Australia & New Zealand.

Katzfey J.J., and Ryan B.F. (1997). 'Modification of the thermodynamic structure of the lower Troposphere by the evaporation of precipitation: A GEWEX cloud system study', *Mon. Wea. Rev.*, **125**, 1431-1446.

Kowalczyk E.A., Garratt J.R., and Krummel P.B. (1991). 'A soil-canopy scheme for use in a numerical model of the atmosphere - 1D stand alone model', CSIRO Atmospheric Research Technical Paper No. 23. 56 pp.

Luhar A.K., Hibberd M.F., and Hurley P.J. (1996). 'Comparison of Closure Schemes used to Specify the Velocity PDF in Lagrangian Stochastic Dispersion Models for Convective Conditions.' *Atmos. Environ.*, **30**, 1407-1418.

Mahrer Y., and Pielke R.A. (1977). 'A numerical study of the airflow over irregular terrain', *Beitr. Phys. Atmosph.*, **50**, 98-113.

Manins P., Carras J. and Williams D. (1992). 'Plume rise from multiple stacks', *Clean Air*, **26**, 65-68.

McGregor J. (1993). 'Economical determination of departure points for semi-Lagrangian Models', *Mon. Wea. Rev.* **121**, 221-230.

McNider R.T., and Pielke R.A. (1981). 'Diurnal boundary-layer development over sloping terrain', *J. Atmos. Sci.*, **38**, 2198-2212.

Mellor G.L., and Yamada T. (1982) 'Development of a turbulence closure model for geophysical fluid problems', *Rev. Geophys. Space Phys.*, **20**, 851-875.

Ng Y., Serebryanikova R. and Wong L. (2000). 'Application of the emissions modelling system EMS-95 to the Victorian Inventory', *Proceedings of the 15th International Clean Air Conference of CASANZ*, Sydney, 26-30 November 2000.

Oke T.R. (1988). 'The urban energy balance', *Progress in Physical Geography*, **12**, 471-508.

Physick W.L. (1994). 'Calculation of dry deposition in LADM', CSIRO Atmospheric Research ECRU Technical Note No. 1.

Physick W.L., Noonan J.A., McGregor J.L., Hurley P.J., Abbs D.J., and Manins P.C. (1994). 'LADM: A Lagrangian Atmospheric Dispersion Model', CSIRO Atmospheric Research Technical Paper No. 24. 137 pp.

Pielke R.A. (1984). 'Mesoscale Meteorological modelling', Academic Press, Orlando, 612 pp.

Puri K., Dietachmayer G.S., Mills G.A., Davidson N.E., Bowen R.A., and Logan L.W. (1998). 'The BMRC Limited Area Prediction System, LAPS', *Aust. Met. Mag.*, **47**, 203-223.

Rikus L. (1993). 'Diagnosing cloud and its interaction with radiation in BMRC GAM', In BMRC Research Report No. 46, Bureau of Meteorology, Australia.

Rodi W. (1985). 'Calculation of stably stratified shear-layer flows with a buoyancy-extended k - ε turbulence model', in J.C.R. Hunt (ed.), *Turbulence and diffusion in stable environments*, Clarendon Press, Oxford, 111-143.

Schulman L., Strimaitis D. and Scire J. (2000). 'Development and evaluation of the PRIME plume rise and building downwash model', *J. Air & Waste Manage. Assoc.*, **50**, 378-390.

Seinfeld J.H., and Pandis S.N. (1998). 'Atmospheric chemistry and physics from air pollution to climate change', Wiley, New York, 1326 pp.

Stauffer D.R., and Seaman N.L. (1994). 'Multiscale four-dimensional data assimilation', *Journal of Applied Meteorology*, **33**, 416-434.

Stephens G.L. (1978). 'Radiation profiles in extended water clouds II : Parameterisation schemes'. *J. Atmos. Sci.*, **35**, 2123-2132.

Venkatram A., Karamchandani P., Prasad P., Sloane C., Saxena P., and Goldstein R. (1997). 'The development of a model to examine source-receptor relationships for visibility on the Colorado Plateau', *Journal of the Air and Waste Management Association*, **47**, 286-301.

Wesley M.L. (1989). 'Parameterisation of surface resistances to gaseous dry deposition in regional-scale numerical models', *Atmos. Environ.*, **23**, 1293-1304.

Appendix

The following summarises the changes (from a technical perspective) made to TAPM in going from V1.0 to V1.4 and from V1.4 to V2.0. Note that the last major release of TAPM was V1.3.1/V1.4 (V1.4 was the same as V1.3.1, except that it allowed access to more regions of synoptic analyses), and the documentation that accompanied this version was for V1.0 with an informal document detailing the changes in going to V1.4.

TAPM V1.4 – Changes from TAPM V1.0

Synoptic-Scale pressure gradients

The synoptic-scale pressure gradient in TAPM was represented via the geostrophic relationship by the terms fu_g and $-fv_g$ in the momentum equations, where u_g and v_g denote the geostrophic wind components. The assumption was made that the wind at each gridpoint of the synoptic analyses, referred to here as the synoptic wind, was the same as the geostrophic wind ($fu_g = fu_s$ and $fv_g = fv_s$), where subscript s denotes the synoptic value. This assumption is no longer used – the synoptic-scale pressure gradient is now directly calculated from the analyses fields. This change led to improved results in a number of verification studies.

Microphysics and Rainfall

An error in the microphysics parameterisation of conversion from cloud water to rain water has been corrected. This error caused underestimation of rainfall.

The approach to including synoptic cloud liquid water into the model has been updated to use a method that is consistent with cloud cover parameterisations in global and synoptic scale models (e.g. see Rikus, 1993). The approach is to enhance the synoptic total water used in the model and entails multiplying the synoptic-scale relative humidity by an enhancement factor. The parameterisation results in no change to the synoptic-scale relative humidity for synoptic relative humidity less than 70% and gives an enhanced value of 100% when the synoptic relative humidity is 85%.

Improved Urban Characterisation

In urban regions the surface temperature, specific humidity and surface fluxes are now calculated using a weighted sum (50/50) of soil/vegetation and urban surface characteristics. Urban surface layer scaling variables are calculated using the same approach as for soil and vegetation, with an urban roughness length of 1 m. Tests of this parameterisation for simulations in both Melbourne and Sydney resulted in improved predictions of near-surface temperature, particularly overnight, where previously the model predictions were usually too low compared to observations.

Gravity-Wave Instability for High Resolution Simulations

In complex terrain near nested grid boundaries, occasional gravity-wave instability can be produced for high resolution simulations (horizontal grid spacing of the order of 300 m). The potential for this problem to occur has now been reduced by decreasing the gravity-wave time-step for grid spacing less than 1000 m.

Plume Rise

Changes have been made to include stack-tip downwash and to modify the final-rise condition to only terminate plume rise when the plume dissipation rate decreases to be less than the ambient dissipation rate.

EGM Mode

In EGM mode on inner grids, the inflow boundary condition could cause a problem for pollution concentrations at the corners of the grid, and these errors could potentially flow onto the grid, corrupting concentration predictions. This problem was usually only important in chemistry mode, and for certain combinations of grid spacing and grid dimensions. This problem has now been corrected.

Biogenic Surface Emissions (.bse file)*

The biogenic surface emissions (*.bse file) array declarations were erroneously using the gridded surface emissions (*.gse file) grid dimensions. This caused problems when using the biogenic surface emissions option, when the biogenic and gridded surface emissions grid dimensions were different. This error has now been corrected.

TAPM V2.0 – Changes from TAPM V1.4

Synoptic-Scale Variations in 3-d

The three-dimensionality of various synoptic-scale fields has now been included in the model. The modifications include

- Latitudinal variation of the zenith angle used in radiation calculations, and the Coriolis parameter used in the momentum equations;
- An option (recommended) to allow synoptic temperature and moisture to vary in 3-d space and time, including the horizontal variation of sea-surface temperature. This should allow better representation/enhancement of synoptic-scale weather patterns. With this option, synoptic winds, temperature and moisture are fed in at the outer-grid boundaries, using the same one-way nesting procedure as for the inner-grids.

Meteorology Scalar Diffusion Coefficient

The scalar diffusion coefficients for water vapour, cloud water and rain water have been modified in order to make them consistent with scalar diffusion in the pollution model.

Check for Numerical Instability in Meteorology

Previously, if TAPM meteorology became numerically unstable, the compiler set variables to Not a Number (NaN), but the simulation continued to run at a much slower rate. This effect has now been bypassed by checking the wind variables and stopping the simulation with an error message if values go outside a realistic range.

Radiation effects of water vapour and carbon dioxide

The effects of water vapour and carbon dioxide on atmospheric heating/cooling rates have now been included for both short-wave and long-wave radiation above the surface (they were already accounted for in the surface radiation).

Clouds and Radiation

A model formulation error in the parameterisation of radiation effects of clouds has been corrected. In cloudy conditions, this problem resulted in short-wave radiation being underestimated and long-wave radiation being overestimated.

Synoptic Cloud

The threshold synoptic-scale relative humidity has been changed from $RH_0 = 70\%$ to $RH_0 = 80\%$, in order to reduce the amount of cloud put into model simulations.

Assimilation of meteorological observations

Assimilation of observed winds at any height can now optionally be included in a simulation.

Fine Particle Matter (FPM)

A new model prognostic variable is now solved for Fine Particle Matter (FPM, notionally $PM_{2.5}$), analogous to that for APM, except that the secondary formation of FPM only receives half of the nitrates (SNGN) that are formed.

Dry Deposition of Particles

The method for calculating the dry deposition velocity of APM and FPM has been modified to use the particle settling velocity and a Quasi-Laminar resistance that accounts for Schmidt number and Stokes number dependencies.

Ambient Turbulence Entrainment in Plume Rise

A preliminary approach to account for the effect of ambient turbulence on plume rise entrainment in V1.4 has been removed. This change makes the model consistent with the usual plume rise formula, which ignores the effects of ambient turbulence on plume rise entrainment, and will lead to slightly higher daytime plume rise.

LPM Mode

The value of the universal constant $C_0 = 2.0$, which is appropriate for laboratory experiments, has been modified to now be $C_0 = 3.0$, to better represent field data (A. Luhar, personal communication, 2001).

First-Order Reaction (Decay) in Tracer Mode

The option to use a first-order decay of pollutant concentration in tracer mode has now been included in both LPM and EGM modes, to allow simple exponential decay of concentration to be used where appropriate.

Rainfall and Wet Deposition

Rainfall and wet deposition processes in the model have now been more closely linked together. The calculation of wet deposition now uses the amount of rain water before it is vertically advected at the rainfall speed for a particular timestep.

Vehicle and Wood Heater Emissions

Five optional gridded surface emission file types have been added to the model, representing emissions at constant temperature for Wood Heater Emissions (WHE), Vehicle Petrol eXhaust emissions (VPX), Vehicle Diesel eXhaust emissions (VDX), Vehicle Lpg eXhaust emissions (VLX) and Vehicle Petrol eVaporative emissions (VPV), with emissions adjusted to model-temperature within each simulation.

Line Source and Area/Volume Source Emissions

Line Source Emissions (LSE) and Area/volume Source Emissions (ASE) in EGM mode are now optionally included.

Building Wakes

The effect of building wakes on point source plume rise and dispersion has now been included, based on the PRIME model.

CSIRO Atmospheric Research Technical Papers

This series was formerly issued as *Division of Atmospheric Research Technical Paper* (nos. 1-19); *CSIRO Division of Atmospheric Research Technical Paper* (nos. 20-37).

No. 1 Galbally, I.E.; Roy, C.R.; O'Brien, R.S.; Ridley, B.A.; Hastie, D.R.; Evans, W.J.F.; McElroy, C.T.; Kerr, J.B.; Hyson, P.; Knight, W.; Laby, J.E. Measurements of trace composition of the Austral stratosphere: chemical and meteorological data. 1983. 31 p.

No. 2 Enting, I.G. Error analysis for parameter estimates from constrained inversion. 1983. 18 p.

No. 3 Enting, I.G.; Pearman, G.I. Refinements to a one-dimensional carbon cycle model. 1983. 35 p.

No. 4 Francey, R.J.; Barbetti, M.; Bird, T.; Beardsmore, D.; Coupland, W.; Dolezal, J.E.; Farquhar, G.D.; Flynn, R.G.; Fraser, P.J.; Gifford, R.M.; Goodman, H.S.; Kunda, B.; McPhail, S.; Nanson, G.; Pearman, G.I.; Richards, N.G.; Sharkey, T.D.; Temple, R.B.; Weir, B. Isotopes in tree rings. 1984. 86 p.

No. 5 Enting, I.G. Techniques for determining surface sources from surface observations of atmospheric constituents. 1984. 30 p.

No. 6 Beardsmore, D.J.; Pearman, G.I.; O'Brien, R.C. The CSIRO (Australia) Atmospheric Carbon Dioxide Monitoring Program: surface data. 1984. 115 p.

No. 7 Scott, J.C. High speed magnetic tape interface for a microcomputer. 1984. 17 p.

No. 8 Galbally, I.E.; Roy, C.R.; Elsworth, C.M.; Rabich, H.A.H. The measurement of nitrogen oxide (NO, NO₂) exchange over plant/soil surfaces. 1985. 23 p.

No. 9 Enting, I.G. A strategy for calibrating atmospheric transport models. 1985. 25 p.

No. 10 O'Brien, D.M. TOVPIX: software for extraction and calibration of TOVS data from the high resolution picture transmission from TIROS-N satellites. 1985. 41 p.

No. 11 Enting, I.G.; Mansbridge, J.V. Description of a two-dimensional atmospheric transport model. 1986. 22 p.

No. 12 Everett, J.R.; O'Brien, D.M.; Davis, T.J. A report on experiments to measure average fibre diameters by optical fourier analysis. 1986. 22 p.

No. 13 Enting, I.G. A signal processing approach to analysing background atmospheric constituent data. 1986. 21 p.

No. 14 Enting, I.G.; Mansbridge, J.V. Preliminary studies with a two-dimensional model using transport fields derived from a GCM. 1987. 47 p.

No. 15 O'Brien, D.M.; Mitchell, R.M. Technical assessment of the joint CSIRO/Bureau of Meteorology proposal for a geostationary imager/ sounder over the Australian region. 1987. 53 p.

No. 16 Galbally, I.E.; Manins, P.C.; Ripari, L.; Bateup, R. A numerical model of the late (ascending) stage of a nuclear fireball. 1987. 89 p.

No. 17 Durre, A.M.; Beer, T. Wind information prediction study: Annaburroo meteorological data analysis. 1989. 30 p. + diskette.

No. 18 Mansbridge, J.V.; Enting, I.G. Sensitivity studies in a two- dimensional atmospheric transport model. 1989. 33 p.

No. 19 O'Brien, D.M.; Mitchell, R.M. Zones of feasibility for retrieval of surface pressure from observations of absorption in the A band of oxygen. 1989. 12 p.

No. 20 Evans, J.L. Envisaged impacts of enhanced greenhouse warming on tropical cyclones in the Australian region. 1990. 31 p. [Out of print]

No. 21 Whetton, P.H.; Pittock, A.B. Australian region intercomparison of the results of some general circulation models used in enhanced greenhouse experiments. 1991. 73 p. [Out of print]

No. 22 Enting, I.G. Calculating future atmospheric CO₂ concentrations. 1991. 32 p.

No. 23 Kowalczyk, E.A.; Garratt, J.R.; Krummel, P.B. A soil-canopy scheme for use in a numerical model of the atmosphere — 1D stand- alone model. 1992. 56 p.

No. 24 Physick, W.L.; Noonan, J.A.; McGregor, J.L.; Hurley, P.J.; Abbs, D.J.; Manins, P.C. LADM: A Lagrangian Atmospheric Dispersion Model. 1994. 137 p.

No. 25 Enting, I.G. Constraining the atmospheric carbon budget: a preliminary assessment. 1992. 28 p.

No. 26 McGregor, J.L.; Gordon, H.B.; Watterson, I.G.; Dix, M.R.; Rotstayn, L.D. The CSIRO 9-level atmospheric general circulation model. 1993. 89 p.

No. 27 Enting, I.G.; Lassey, K.R. Projections of future CO₂. with appendix by R.A. Houghton. 1993. 42 p.

No. 28 [Not published]

No. 29 Enting, I.G.; Trudinger, C.M.; Francey, R.J.; Granek, H. Synthesis inversion of atmospheric CO₂ using the GISS tracer transport model. 1993. 44 p.

No. 30 O'Brien, D.M. Radiation fluxes and cloud amounts predicted by the CSIRO nine level GCM and observed by ERBE and ISCCP. 1993. 37 p.

No. 31 Enting, I.G.; Wigley, T.M.L.; Heimann, M. Future emissions and concentrations of carbon dioxide: key ocean/atmosphere/land analyses. 1994. 120 p.

No. 32 Kowalczyk, E.A.; Garratt, J.R.; Krummel, P.B. Implementation of a soil-canopy scheme into the CSIRO GCM — regional aspects of the model response. 1994. 59 p.

No. 33 Prata, A.J. Validation data for land surface temperature determination from satellites. 1994. 40 p.

No. 34 Dilley, A.C.; Elsum, C.C. Improved AVHRR data navigation using automated land feature recognition to correct a satellite orbital model. 1994. 22 p.

No. 35 Hill, R.H.; Long, A.B. The CSIRO dual-frequency microwave radiometer. 1995. 16 p.

No. 36 Rayner, P.J.; Law, R.M. A comparison of modelled responses to prescribed CO₂ sources. 1995. 84 p.

No. 37 Hennessy, K.J. CSIRO Climate change output. 1998. 23 p.

No. 38 Enting, I. G. Attribution of greenhouse gas emissions, concentrations and radiative forcing. 1998. 29 p.

No. 39 O'Brien, D.M.; Tregoning, P. Geographical distributions of occultations of GPS satellites viewed from a low earth orbiting satellite. 1998. 23 p.

No. 40 Enting, I. G. Characterising the temporal variability of the global carbon cycle. 1999. 23 p.

No. 41 [Not published]

No. 42 Mitchell, R. M. Calibration Status of the NOAA AVHRR Solar Reflectance Channels: CalWatch Revision 1. 1999. 20 p.

No. 43 Hurley, P.J. The Air Pollution Model (TAPM) Version 1: technical description and examples. 1999. 41 p.

No. 44 Frederiksen, J.S.; Dix, M.R.; Davies, A.G. A new eddy diffusion parameterisation for the CSIRO GCM. 2000. 31 p.

No. 45 [Not published]

No. 46 Prata, A.J. Global Distribution of Maximum Land Surface Temperature Inferred from Satellites: Implications for the Advanced Along Tracking Scan Radiometer. 2000. 30 p. Electronic edition only.

No. 47 Prata, A.J. Precipitable water retrieval from multi-filtered shadowband radiometer measurements. 2000. 14 p. Electronic edition only.

No. 48 Prata, A.J., Grant, I.F. Determination of mass loadings and plume heights of volcanic ash clouds from satellite data. 2001. 39 p. Electronic edition only.

No. 49 O'Brien, D.M. Numerical calculation of the transfer of polarized radiation by a scattering and absorbing atmosphere. 2001. 65 p. Electronic edition only.

No. 50 R.L. Law, Vohralik, P.F. Methane sources from mass-balance inversions: Sensitivity to transport. 2001 27p.

No. 51 Meyer, C.P., Galbally, I.E., Wang, Y.P., Weeks, I.A., Jamie, I., Griffith, D.W.T., Two automatic chamber techniques for measuring soil-atmosphere exchanges of trace gases and results of their use in the OASIS field experiment. 2001 33 p.

No. 52 Mitchell, R.M. In-flight characteristics of the space count of NOAA AVHRR channels 1 and 2. 2001 24 p.

No. 53 Young, S.A. An investigation into the performance of algorithms used to retrieve cloud parameters from LITE lidar data, and implications for their use with PICASSO-CENA lidar data.

Address and Contact Details:

CSIRO Atmospheric Research
Private Bag No.1 Aspendale Victoria 3195 Australia
Ph: (+61 3) 9239 4400; fax: (+61 3) 9239 4444
e-mail: chief@csiro.au